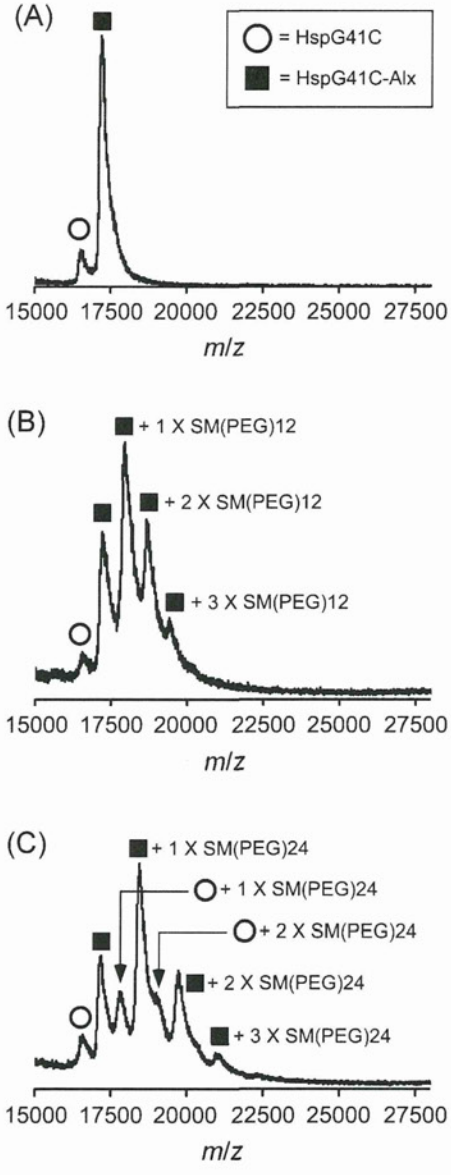

Figure 2. MALDI-ToF MS analyses of (A) HspG41C-Alx, (B) HspG41C-Alx-SM(PEG)$_{12}$, and (C) HspG41C-Alx-SM(PEG)$_{24}$. Open circles and filled squares indicate HspG41C- and HspG41C-derived peaks, respectively. Theoretical molecular weight of HspG41C and HspG41C-Alx were 16498 g/mol and 17219 g/mol, respectively. Net mass addition through conjugation of one SM(PEG)$_{12}$ and one SM(PEG)$_{24}$ molecule with protein cages were 750 g/mol and 1279 g/mol, respectively.

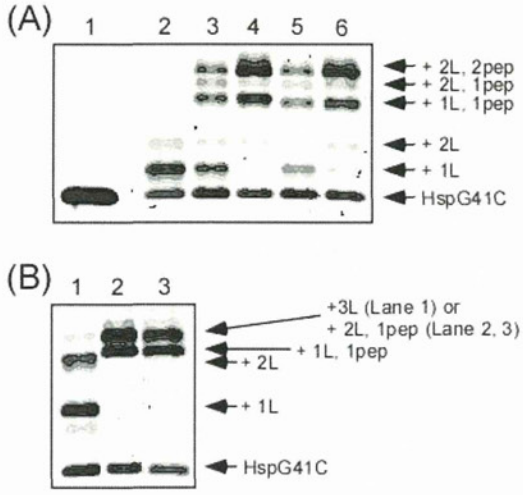

Figure 3. SDS-PAGE analyses of HspG41C–SP94-peptide conjugates. (A) HspG41C-Alx-SM(PEG)$_{12}$–SP94 peptide conjugates. Lane 1, HspG41C-Alx; lane 2, HspG41C-Alx-SM(PEG)$_{12}$; lane 3, 12-N(1); lane 4, 12-N(2); lane 5, 12-C(1); and lane 6, 12-C(2). (B) HspG41C-Alx-SM(PEG)$_{24}$–SP94 peptide conjugates. Lane 1, HspG41C-Alx-SM(PEG)$_{24}$; lane 2, 24-N(1); and lane 3, 24-C(1). Each band was imaged by fluorescence from Alexa488 conjugated with protein cages. "L" and "pep" indicate SM(PEG)$_n$ linker and SP94 peptide, respectively.

To introduce the maleimide groups into HspG41C-Alx, heterobifunctional linkers (SM(PEG)$_{12}$ or SM(PEG)$_{24}$) that possessed NHS ester and maleimide groups at either side of the linkers were conjugated to HspG41C-Alx thorough amide bonds to obtain HspG41C-Alx-SM(PEG)$_n$. MALDI-ToF MS analyses showed that 1–3 molecules of the linker were bound to HspG41C-Alx-SM(PEG)$_n$ (Figure 2B,C). Moreover, these corresponding bands were observed from SDS-PAGE analysis (Figure 3). SDS-PAGE analyses revealed that, on average, 23 ± 2 molecules of SM(PEG)$_{12}$ and 23 ± 3 molecules of SM(PEG)$_{24}$ were bound to HspG41C-Alx-SM(PEG)$_{12}$ and HspG41C-Alx-SM(PEG)$_{24}$, respectively (Figure 3).

To conjugate SP94 peptides into HspG41C-Alx-SM(PEG)$_n$, two SP94 peptide derivatives containing a Cys residue at the N-terminus or the C-terminus of the original SP94 peptide sequences were prepared, i.e., peptide **1** and peptide **2** possessed a Cys residue at the N-terminus and the C-terminus of the original SP94 peptide sequences, respectively. Peptide **1** or **2** was modified with HspG41C-Alx-SM(PEG)$_n$ through a Michael addition reaction between a thiol group of a SP94 peptide derivative and maleimide groups of HspG41C-Alx-SM(PEG)$_n$. SDS-PAGE analyses revealed that peptides **1** and **2** were successfully modified with HspG41C-Alx-SM(PEG)$_{12}$ because three new bands corresponding to HspG41C-Alx-SM(PEG)$_{12}$ bound to one or two SP94 peptide molecules per protein monomer were observed (lanes 3–6) (Figure 3A). Moreover, one SP94 peptide per protein monomer could conjugate into HspG41C-Alx-SM(PEG)$_{24}$ (Figure 3B). Average SP94 peptide contents in each HspG41C-Alx-SM(PEG)$_n$ were determined from SDS-PAGE analyses (Figure 3) and are summarized in Table 1.

Size Measurements of Linker- and Peptide-Modified HspG41C. Sizes of HspG41C conjugates in PBS were measured by DLS analyses. HspG41C is known to form a cage structure with a diameter of 12 nm.[10] As shown in Figure 4A, HspG41C used in the present study also showed a comparable size. After conjugation of SM(PEG)$_n$ linkers to HspG41C, the size distribution peak of HspG41C-SM(PEG)$_n$ was slightly shifted to a larger size when compared with that of HspG41C. However, both of HspG41C-SM(PEG)$_n$ did not form any large aggregates (>100 nm) (Figure 4A, inset).

As shown in Figure 4B, the size distribution peak of all HspG41C-SM(PEG)$_{12}$-SP94 peptide conjugates are slightly shifted to a larger size when compared with that of their precursor (HspG41C-SM(PEG)$_{12}$). Same trends were detected from the system of HspG41C-SM(PEG)$_{24}$-SP94 peptide conjugates (Figure 4C). On the other hand, all of the HspG41C-SM(PEG)$_n$-SP94 peptide conjugates did not show any large aggregate formations (>100 nm) (Figure 4B,C, inset).

dx.doi.org/10.1021/bc300015f | Bioconjugate Chem. 2012, 23, 1494–1501

Table 1. Characterization of HspG41C-SP94 Peptide Conjugates Used in This Study

sample[a]	peptide number/cage[b]	conjugated peptide[c]
12-N(1)	12 ± 2	1
12-N(2)	23 ± 2	1
12-C(1)	13 ± 2	2
12-C(2)	22 ± 3	2
24-N(1)	15 ± 2	1
24-C(1)	16 ± 1	2

[a]Numbers 12 and 24 indicate HspG41C-SP94 peptide conjugates using HspG41C-Alx-SM(PEG)$_{12}$ and HspG41C-Alx-SM(PEG)$_{24}$ as the precursors, respectively. N and C mean SP94 peptides containing a Cys residue at the N-terminus and C-terminus, respectively. Furthermore, parenthesized number 1 and 2 exhibit the addition of 2 and 10 equiv of SP94 peptides to HspG41C-Alx-SM(PEG)$_n$, respectively, when synthesizing them. [b]SP94 peptide contents of each cage were calculated from the results of SDS-PAGE analyses. Data are means ± SD of three independent experiments. [c]Sequences of peptides **1** and **2** were Ac-CGGSFSIIHTPILPL-NH_2 and Ac-SFSIIHTPILPLGGC-NH_2, respectively.

These results showed that the cage structure of HspG41C was sufficiently robust for chemical modification of target peptides.

Fluorescence Microscopic Observation of Cellular Binding of HspG41C-SM(PEG)$_n$-SP94 Peptide Conjugates toward Various Kinds of Cell Lines. To verify if HspG41C-SM(PEG)$_n$-SP94 peptide conjugates could bind selectively to HCC cells, Alexa488-labeled conjugates were added to human HCC cell lines (Huh-7 and HepG2), HeLa and RLN-8, and binding of conjugates to cells was then detected using a fluorescence microscope. When Alexa488-labeled HspG41C-SM(PEG)$_n$-SP94 peptide conjugates were added to Huh-7 and HepG2 cells, green fluorescence was observed, indicating that all conjugates could bind the human HCC-derived cell lines (Figure 5A). However, of the number of protein cages bound to HCC cells changed appreciably according to (i) SP94 peptide content, (ii) conjugation site of the SP94 peptide, and (iii) linker length, which will be discussed later. In contrast to HCC-derived cells, obvious green fluorescence was not detected after addition of Alexa488-labeled HspG41C-SM(PEG)$_n$-SP94 peptide conjugates to the other cell lines (HeLa and RLN-8 cells). These results showed that HspG41C-SM(PEG)$_n$-SP94 peptide conjugates could bind selectively to human HCC-derived cell lines.

Influence of SP94 Peptide Content in HspG41C-SM(PEG)$_n$-SP94 Peptide Conjugates on Cellular Binding. To clarify whether SP94 peptide content in HspG41C-SM(PEG)$_n$-SP94 peptide conjugates affected cellular binding, the fluorescence intensity of cellular lysates was compared 24 h after the addition of Alexa-labeled conjugates to HepG2 and Huh-7cells. When 12-N(2) (23 peptides/cage) and 12-N(1) (12 peptides/cage), both of which were modified SP94 peptides at the N-terminus of SP94 peptides, were added to HepG2 cells, 12-N(2) showed 3.9× higher fluorescence intensity than 12-N(1) (Figure 5B). Moreover, 2.7× higher fluorescence intensity from 12-C(2) (22 peptides/cage) was observed when compared with that from 12-C(1) (13 peptides/cage) (Figure 5B). Similarly, an increase in SP94 peptide content in conjugates increased fluorescence intensity in Huh-7 cells, but their variances (~1.5× higher) in Huh-7 cells were slightly lower than those in HepG2 cells (Figure 5C). Similarly, one study reported that SP94 peptide-displayed liposomes increased their binding to HCC cells with increasing

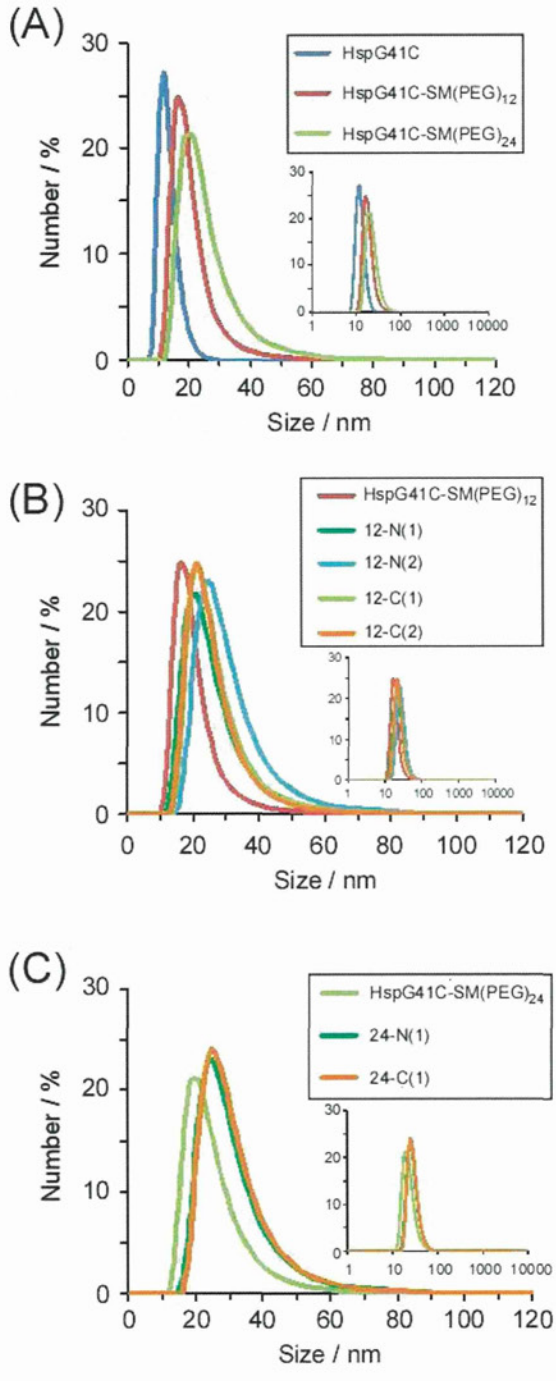

Figure 4. Size distributions of (A) HspG41C-SM(PEG)$_n$, (B) HspG41C-SM(PEG)$_{12}$-SP94 peptide conjugates, and (C) HspG41C-SM(PEG)$_{24}$-SP94 peptide conjugates determined by DLS. Measurements were undertaken at least twice, and the results showed almost identical size distributions.

SP94 peptide numbers on liposomes.[9] Therefore, we concluded that an increase in SP94 peptide levels in conjugates could increase the binding of conjugates toward HCC cells due to the multivalent interaction of conjugates.

Influence of SP94 Peptide Conjugation Site (N- or C-Terminus) in Conjugates upon Cellular Binding. One study suggested that the C-terminal region of SP94 peptide is essential for the binding of HCC cells (SFSIIHTPILPL; consensus sequence shown in under-lined segment).[8] Thus, we investigated whether the SP94 peptide conjugation site on

dx.doi.org/10.1021/bc300015f | Bioconjugate Chem. 2012, 23, 1494–1501

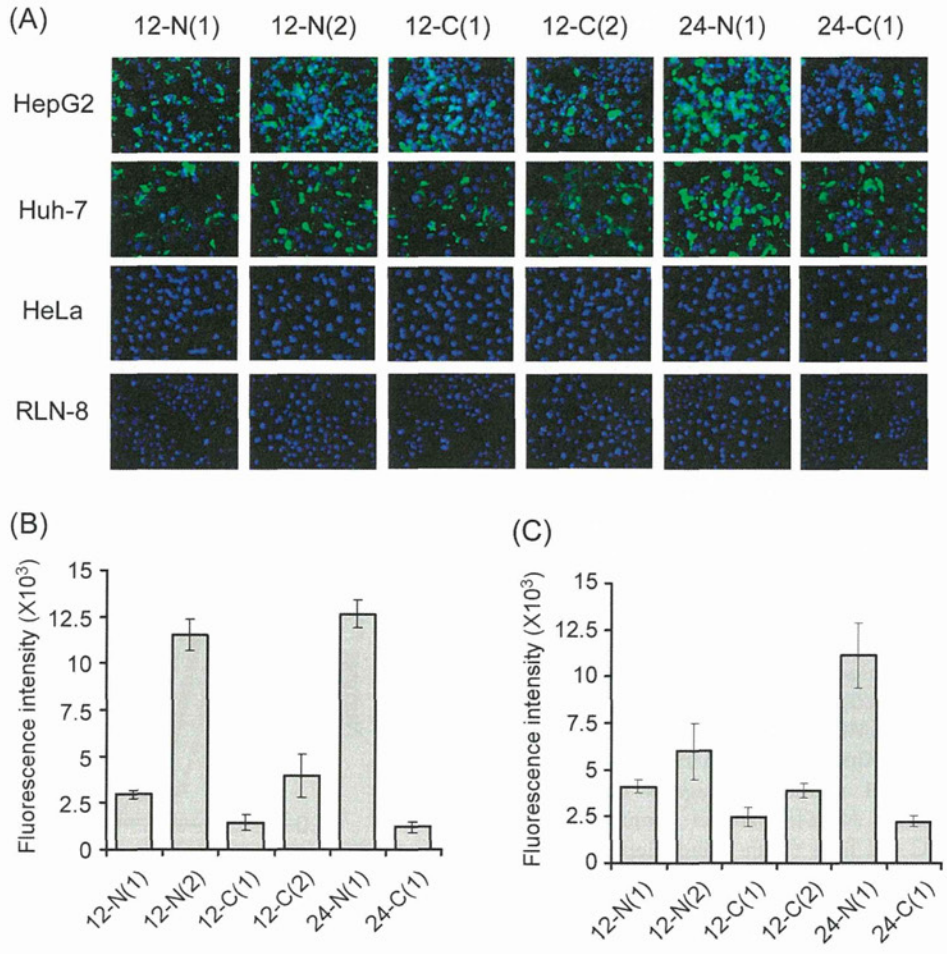

Figure 5. (A) Fluorescence microscopic observation of the uptake of each HspG41C-SM(PEG)$_n$–SP94. Images were obtained 24 h after addition of 40 nM of HspG41C-SM(PEG)$_n$–SP94. Green (Alexa488) and blue (Hoechst 33342) colors indicate HspG41C-SM(PEG)$_n$–SP94 and the nucleus, respectively. Experiments were undertaken at least thrice. Fluorescence intensity in (B) HepG2 and (C) Huh-7 cells after addition of each HspG41C-SM(PEG)$_n$–SP94. Twenty-four hours after the addition of 4 nM of protein cages, cells were lysed in lysis buffer (20 mM Tris-HCl, 2 mM EDTA, and 0.05% Triton-X 100 at pH 7.4), and the fluorescence intensity of lysate solution measured using a microplate reader. Data are means ± SD of three independent experiments.

protein cages (i.e., N- or C-terminal of SP94 peptide) could the affect affinity of SP94-modified cages toward HCC cells using each conjugate, which had identical peptide content and linker length, but a different SP94 peptide conjugation site. Protein cages modified by the N-terminal of SP94 peptide (12-N(1), 12-N(2), and 24-N(1)) showed 2–11× higher fluorescence intensity in HepG2 cells compared with those on the C-terminal of SP94 peptide (12-C(1), 12-C(2), and 24-C(1)) (i.e., 2.1× for 12-N(1) vs 12-C(1), 2.9× for 12-N(2) vs 12-C(2), and 11× for 24-N(1) vs 24-C(1)) (Figure 5B). Similar results were observed in Huh-7 cells (Figure 5C). These results strongly suggested that, with respect to cell binding, the SP94 peptide bound to a protein cage at the N-terminus of peptides was superior to that at the C-terminus of peptides in cell binding because C-terminal region of SP94 peptide is indispensable to its binding to HCC cells.

Influence of Linker Length between Protein Cage and SP94 Peptide upon Cellular Binding. To investigate the effect of linker length between cages and SP94 peptides upon the affinity of engineered cages against HCC cells, the fluorescence intensity of HCC cells was measured after addition of 12-N(1) and 24-N(1) with different numbers of SP94 peptide to HCC cells. The 24-N(1) containing longer linkers showed 4.3× higher fluorescence intensity than 12-N(1) in HepG2 cells (Figure 5B). Similarly, a 2.7× higher fluorescence intensity in Huh-7 cells was detected from 24-N(1) compared with 12-N(1) (Figure 5C). These results suggested that a SP94-modified cage through a longer linker was superior in binding to HCC cells, because a longer linker is more flexible, which can make binding of cages to cells easier. Interestingly, 12-C(1) and 24-C(1) exhibited almost comparable fluorescence intensity after their addition into HCC cells. This observation suggested that linker length affects affinity of cages toward HCC cell only when SP94 peptide is modified with protein cages at N-terminus.

Cellular Uptake Mechanisms and Subcellular Localization of HspG41C-SM(PEG)$_n$-SP94 Peptide Conjugates. To verify cellular uptake mechanisms of HspG41C-SM(PEG)-SP94 peptide conjugates, Alexa-modified SP94-Hsp cages (40 nM of 12-N(1) or 24-N(1)) were transfected into Huh-7 cells with excessive amounts of free SP94 peptides (100 μM). Free SP94 peptides showed no effect on the viability of Huh-7 cells at concentrations of <300 μM (Figure 6A). As shown in Figure 5A, 12-N(1) and 24-N(1) were effectively taken up by Huh-7 cells, but their uptakes were dramatically reduced after adding excessive amounts of free SP94 peptides that block the binding of 12-N(1) and 24-N(1) to target receptors (Figure 6B). These

dx.doi.org/10.1021/bc300015f | Bioconjugate Chem. 2012, 23, 1494–1501

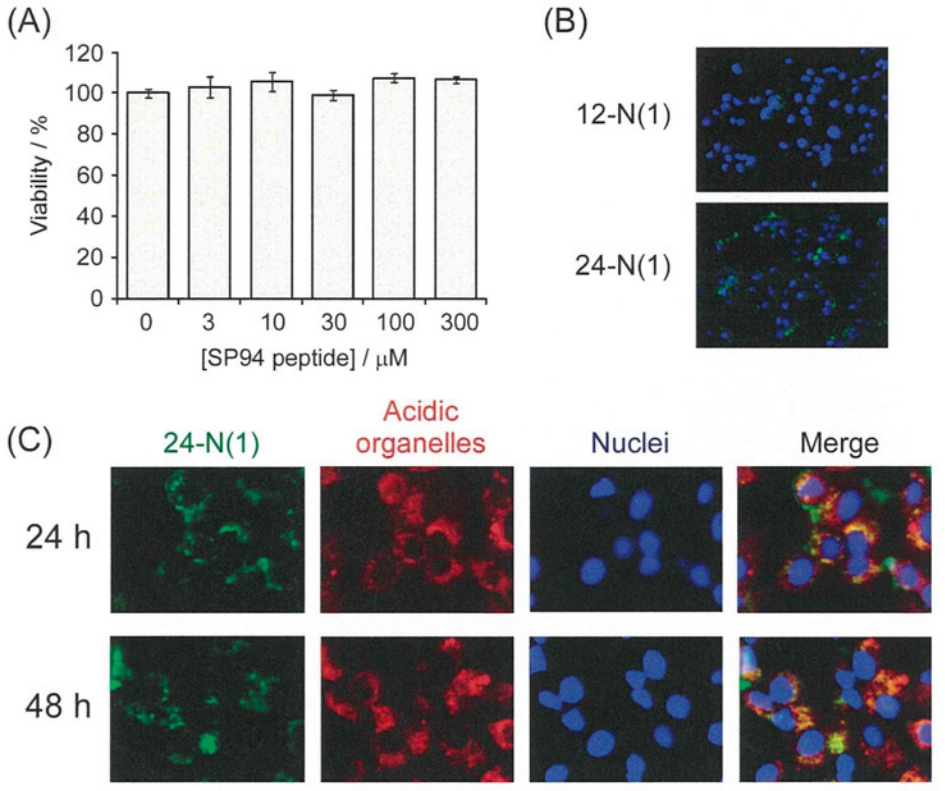

Figure 6. (A) Cytotoxicity of free SP94 peptides toward Huh-7 cells. Data are means ± SEM of three independent experiments. (B) Uptake of HspG41C-SM(PEG)$_n$-SP94 (40 nM) by Huh-7 cells after adding excessive amounts of free SP94 peptides (100 μM). (C) Subcellular localization of 24-N(1) in Huh-7 cells. Acidic organelles (red) and nuclei (blue) were stained by LysoTracker-Red and Hoechst 33342, respectively. Overlapping of 24-N(1) with acidic organelles resulted in yellow fluorescence in the merged pictures.

results show that 12-N(1) and 24-N(1) are taken up by Huh-7 cells through receptor-mediated endocytosis.

Intracellular localization of HspG41C-SM(PEG)$_n$-SP94 peptide conjugates (24-N(1)) was examined using a fluorescence microscopy. Cellular acidic organelles (endosomes/lysosomes) and nuclei were stained by LysoTracker-Red and Hoechst 33342, respectively. Twenty-four hours after adding 24-N(1) conjugates (green) to Huh-7 cells, most of them localized in acidic organelles (red), which was shown in yellow fluorescence in the merged pictures. Furthermore, the 24-N(1) conjugates were still localized in acidic organelles even at 48 h post-transfection (Figure 6C).

■ CONCLUSION

We synthesized an SP94 peptide-modified protein cage (HspG41C-SM(PEG)$_n$-SP94) that could bind selectively to HCC-derived cell lines. An increase in SP94 peptide contents in engineered cages elevated the affinity of cages to HCC cells (especially HepG2 cells). In addition, protein cages modified by the N-terminus of SP94 peptides showed higher cellular uptake than those modified by the C-terminus. Moreover, an increase in linker length between protein cages and SP94 peptide increased the affinity of conjugates to HCC cells. Collectively, a protein cage modified by the N-terminus of SP94 peptide through a longer linker molecule and containing high SP94 peptide levels showed the most effective binding toward HCC cells. These observations could be helpful for developing DDS carriers and imaging systems based on the targeting of peptide ligands. Furthermore, an SP94 peptide-modified Hsp cage will be an effective DDS carriers and imaging device toward HCC cells.

■ AUTHOR INFORMATION

Corresponding Author

*Tel: +81-92-642-6251. Fax: +81-92-642-6252. E-mail: m-murata@dem.med.kyushu-u.ac.jp.

Present Address

⊥Department of Applied Chemistry, Graduate School of Engineering, Osaka University, 2−1 Yamadaoka, Suita, Osaka 565−0871, Japan.

Notes

The authors declare no competing financial interest.

■ ACKNOWLEDGMENTS

This work was supported financially by a Health Labour Sciences Research Grant (Research on Publicly Essential Drugs and Medical Devices) from the Ministry of Health Labour and Welfare of Japan, and Grant-in-Aid for Scientific Research (no. 21300190, no. 23650288) from the Ministry of Education, Culture, Sports, Science and Technology of Japan, and Grant-in-Aid for Research Activity Start-up (no. 23800045) from the MEXT of Japan.

■ REFERENCES

(1) Siegel, R., Ward, E., Brawley, O., and Jemal, A. (2011) Cancer statics, 2011: the impact of eliminating socioeconomic and radical disparities on premature cancer deaths. *CA Cancer J. Clin. 61*, 212−236.

(2) Llovet, J. M., and Bruix, J. (2008) Molecular targeted therapies in hepatocellular carcinoma. *Hepatology 48*, 1312−1327.

(3) Thomas, M. (2009) Molecular targeted therapy for hepatocellular carcinoma. *J. Gastroenterol. 44*, 136−141.

(4) Finn, R. S. (2010) Development of molecularly targeted therapies in hepatocellular carcinoma: where do we go now? *Clin. Cancer Res. 16,* 390−397.
(5) Byrne, J. D., Betancourt, T., and Brannon-Peppas, L. (2008) Active targeting schemes for nanoparticle systems in cancer therapeutics. *Adv. Drug Delivery Rev. 60,* 1615−1626.
(6) Shimoda, A., Sawada, S., and Akiyoshi, K. (2011) Cell specific peptide conjugated polysaccharide nanogels for protein delivery. *Macromol. Biosci. 11,* 882−888.
(7) Allen, T. M. (2002) Ligand-targeted therapeutics in anticancer therapy. *Nat. Rev. Cancer 2,* 750−763.
(8) Lo, A., Lin, C. T., and Wu, H. C. (2008) Hepatocellular carcinoma cell-specific peptide ligand for targeted drug delivery. *Mol. Cancer Ther. 7,* 579−589.
(9) Ashley, C. E., Carnes, E. C., Phillips, G. K., Padilla, D., Durfee, P. N., Brown, P. A., Hanna, T. N., Liu, J., Phillips, B., Carter, M. B., Carroll, N. J., Jiang, X., Dunphy, D. R., William, C. L., Petsev, D. N., Evans, D. G., Parikh, A. N., Chackerian, B., Wharton, W., Peabody, D. S., and Brinker, C. J. (2011) The targeted delivery of multicomponent cargos to cancer cells by nanoporous particles-supported lipid bilayers. *Nat. Mater. 10,* 389−397.
(10) Kim, K. K., Kim, R., and Kim, S. H. (1998) Crystal structure of a small heat-shock protein. *Nature 394,* 595−599.
(11) Flenniken, M. L., Liepold, L. O., Crowley, B. E., Willits, D. A., Young, M. J., and Douglas, T. (2005) Selective attachment and release of a chemotherapeutic agent from the interior of a protein cage architecture. *Chem. Commun.,* 447−449.
(12) Varpness, Z., Suci, P. A., Ensign, D., Young, M. J., and Douglas, T. (2009) Photosensitizer efficiency in genetically modified protein cage architectures. *Chem. Commun.,* 3726−3728.
(13) Liepold, L. O., Abedin, M. J., Buckhouse, E. D., Frank, J. A., Young, M. J., and Douglas, T. (2009) Supramolecular protein cage composite MR contrast agents with extremely efficient relaxivity properties. *Nano Lett. 9,* 4520−4526.
(14) Uchida, M., Kosuge, H., Terashima, M., Willits, D. A., Liepold, L. O., Young, M. J., McConnell, M. V., and Douglas, T. (2011) Protein cage nanoparticles bearing the LyP-1 peptide for enhanced imaging of macrophage-rich vascular lesions. *ACS Nano 5,* 2493−2502.
(15) Choi, S. H., Kwon, I. C., Hwang, K. Y., Kim, I. S., and Ahn, H. J. (2011) Small heat shock protein as a multifunctional scaffold: integrated tumor targeting and caspase imaging within a single cage. *Biomacromolecules 12,* 3099−3106.
(16) Sao, K., Murata, M., Umezaki, K., Fujisaki, Y., Mori, T., Niidome, T., Katayama, Y., and Hashizume, M. (2009) Molecular design of protein-based nanocapsules for stimulus-responsive characteristics. *Bioorg. Med. Chem. 17,* 85−93.
(17) Sao, K., Murata, M., Fujisaki, Y., Umezaki, K., Mori, T., Niidome, T., Katayama, Y., and Hashizume, M. (2009) A novel protease activity assay using a protease-responsive chaperone protein. *Biochem. Biophys. Res. Commun. 383,* 293−297.
(18) Flenniken, M. L., Willits, D. A., Brumfield, S., Young, M. J., and Douglas, T. (2003) The small heat shock protein cage from *Methanococcus jannaschii* is a versatile nanoscale platform for genetic and chemical modification. *Nano Lett. 3,* 1573−1576.
(19) Flenniken, M. L., Willits, D. A., Harmsen, A. L., Liepold, L. O., Harmsen, A. G., Young, M. J., and Douglas, T. (2006) Melanoma and lymphocyte cell-specific targeting incorporated into a heat shock protein cage architecture. *Chem. Biol. 13,* 161−170.
(20) Flenniken, M. L., Uchida, M., Liepold, L. O., Kang, S., Young, M. J., and Douglas, T. (2009) A library of protein cage architectures as nanomaterials. *Curr. Top. Microbiol. Immunol. 327,* 71−93.
(21) Kovacs, E. W., Hooker, J. M., Romanini, D. W., Holder, P. G., Berry, K. E., and Francis, M. B. (2007) Dual-surface-modified bacteriophage MS2 as an ideal scaffold for a viral capsid-based drug delivery system. *Bioconjugate Chem. 18,* 1140−1147.

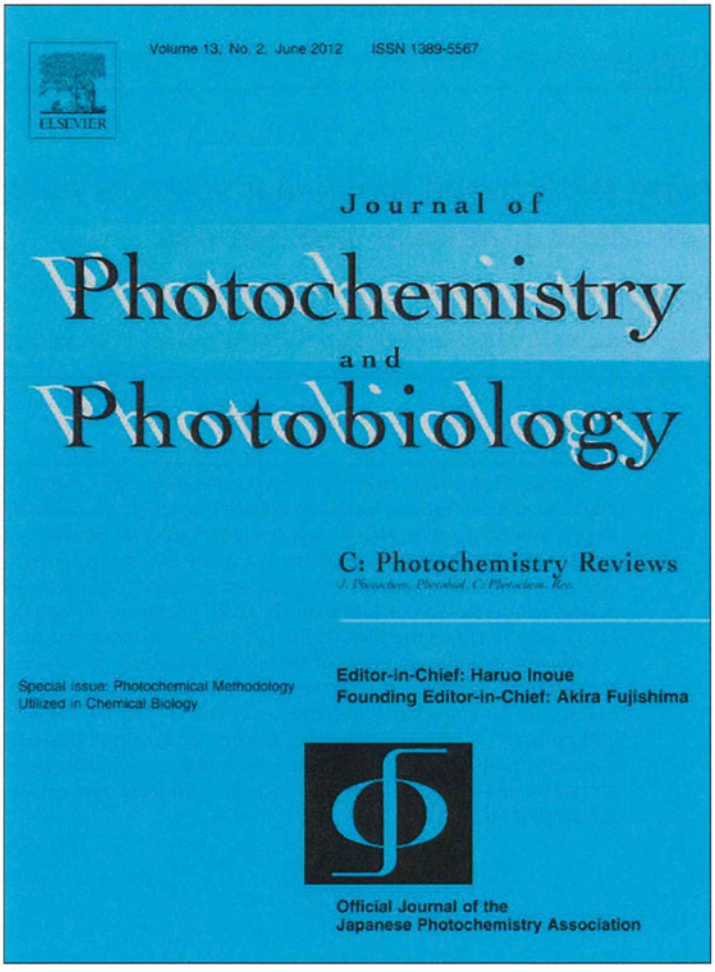

Journal of Photochemistry and Photobiology C: Photochemistry Reviews 13 (2012) 148–167

Contents lists available at SciVerse ScienceDirect

Journal of Photochemistry and Photobiology C: Photochemistry Reviews

journal homepage: www.elsevier.com/locate/jphotochemrev

Invited review

Photochemically relevant DNA-based molecular systems enabling chemical and signal transductions and their analytical applications

Toshihiro Ihara*, Yusuke Kitamura

Department of Applied Chemistry and Biochemistry, Graduate School of Science and Technology, Kumamoto University, 2-39-1 Kurokami, Chuo-ku, Kumamoto 860-8555, Japan

ARTICLE INFO

Article history:
Received 31 January 2012
Received in revised form 16 March 2012
Accepted 21 March 2012
Available online 30 March 2012

Keywords:
DNA
Oligonucleotide
Allosterism
Functional DNA
Ribozyme
DNAzyme
Aptamer
Metal base pair
Assembly
DNA machine
DNA device
Bioorthogonal reaction
Staudinger reaction
Click chemistry
Fluorescence
Conductivity
Photochemical ligation

ABSTRACT

In biology, DNA is the central molecule that stores the genetic information. DNA also has attractive physicochemical features for use as materials in molecular assemblies. DNA is chemically stable and can be prepared in nearly any length and sequence by chemical and enzymatic syntheses. Auxiliary functional groups can be built into the backbone as amidite reagents using automated DNA synthesizers. In addition, we can choose an appropriate method from abundant chemistries for post-modifications. The structures of DNA complexes can be rationally designed by bottom-up self-assembly. Therefore, functional groups can be positioned on the DNA scaffold in distinct distance and spatial arrangements.

In the last decade, a number of DNA-based allosteric molecular systems have been reported. Some of the systems function as signal transducers, amplifiers, and chemical catalysts. These systems are rather exciting as fundamental achievements of the studies for nanomachines or nanodevices. They should also be useful as robust molecular sensors for sensitive bioassays. In this review, we will cover the photochemically relevant DNA-based molecular systems. They are classified into three groups: (i) DNA-templated molecular/ion assemblies; (ii) DNA-directed complexation; and (iii) chemical transformations accelerated on DNA.

Contents

* Corresponding author. Tel.: +81 96 342 3873; fax: +81 96 342 3873.
E-mail address: toshi@chem.kumamoto-u.ac.jp (T. Ihara).

1389-5567/$20.00 © 2012 Elsevier B.V. All rights reserved.
http://dx.doi.org/10.1016/j.jphotochemrev.2012.03.002

Toshihiro Ihara, Professor of Department of Applied Chemistry and Biochemistry, Graduate School of Science and Technology, Kumamoto University. He was born in Miyazaki, Japan. After receiving his Bachelor (1988), Master (1990), and Doctor (1993) degrees from Kyushu University under the supervision of Prof. M. Takagi, he took a position as Research Associate at the Department of Chemical Science and Technology, Kyushu University (1993–1996). In 1996, he joined Kumamoto University as a Lecturer and has been Professor since 2009. His research interests focus on genome chemistries, especially on the details of their molecular recognition and application in analytical sciences.

Yusuke Kitamura, Assistant Professor of the Department of Applied Chemistry and Biochemistry, Graduate School of Science and Technology, Kumamoto University. He was born in Nagasaki, Japan. After receiving his Bachelor (2001), Master (2003), and Doctor (2006) degrees from Kumamoto University under the supervision of Prof. T. Ihara and Prof. A. Jyo, he spend 1 year (2006–2007) at Kumamoto University as a postdoctoral fellow. Subsequently, he took a position as an Assistant Professor at the Department of Applied Chemistry, Chuo University (2007–2011). In 2011, he joined Kumamoto University as an Assistant Professor. His research interests include nucleic acid chemistry, particularly discovery of new DNA-based fluorophores, sensors, artificial enzymes, and architectures.

1. Introduction

All living organisms share nucleic acid as common genetic material. The nucleobase sequence of DNA stores and imparts genetic instructions, whereas RNA functions as a messenger and regulator of gene expression. The elucidation of the 3D structure of DNA in 1953 by Watson and Crick provided a significant boost to biological research [1]. Intensive studies over nearly six decades have made revolutionary progress in our understanding of biology, and the impetus of further characterization of biological processes continues unabated. With the efforts of genome sequencing [2,3], significant advances in biology have contributed not only to medicinal and diagnostic sciences but also to other fields including archaeology, evolution, parentage testing, and forensic science [4].

Besides the significance of DNA in biological processes, scientists have found various uses for DNA within completely non-biological context [5,6]. Some of the fundamental techniques developed in molecular biology including DNA chemical synthesis and PCR (polymerase chain reaction) enable researchers to use DNA as chemical components in elaborate DNA nanostructures. A deep understanding of the mechanical and chemical properties of DNA and the physical chemistry associated with DNA hybridization were also essential for developing the research field of DNA nanostructures. DNA origami is one of the typical achievements in this field of research [7,8]. As the independent line in the nucleic acids sciences, functional nucleic acids such as aptamers, ribozymes, and other allosteric DNA molecular systems have been developed in 1990s [9,10]. These techniques added dynamic or allosteric features to DNA nanostructures such that these compounds could be used as switchable molecular systems that are applicable as molecular sensing devices. That is, the functional nucleic acids merged biology with DNA nanotechnology to realize DNA nanomachines or nanodevices [9–12]. The molecular beacon (MB) is one of the most successful nanodevices [13,14]. The design concept of the MB is flexible. It is based on a reversible structural transformation in response to a specific target DNA. The MB is recognized as an important motif of nanodevices and is commonly used as a part of more complex molecular systems.

Controlled alignment of auxiliary functional groups (i.e., non-biological molecules with fluorescent character, electronic properties, or specific chemical activity) on biomolecular scaffolds such as nucleic acids and proteins has been investigated for the design of catalysts for specific reactions or as probes that response to specific chemical or physical stimuli. Recently, several DNA-directed molecular assemblies with cooperatively developed functions have been reported [15–17]. DNA is chemically stable and the techniques used to synthesize DNA (chemical and enzymatic) have matured. Therefore, various chemical groups can be covalently introduced into DNA to obtain DNA conjugates with desired artificial functions. The programmability and switchable (reversible) nature of specific DNA structures as scaffolds enable us to form supramolecular complexes in which several functional groups or split functions are brought together with defined distances and spatial orientations. If reversible binary motion of the functional groups on DNA is controlled by specific stimuli the DNA assemblies act as allosteric nanodevices for chemical or signal transformation processes (Fig. 1).

Among such DNA-based functional molecular assemblies, we have focused on systems that accelerate specific chemical transformations that are promoted by light and that produce optically or electrically active products. Each specific structure of DNA such as hairpins, duplexes, triplexes, and quadruplexes require particular conditions (e.g., pH, ionic strength, temperature etc.) to maintain their native structure in aqueous solution. Therefore, built-in and designed reactions on these DNA-based assemblies should involve reactions that proceed efficiently in aqueous media under mild conditions. Several bioorthogonal chemical reactions have been recently developed [18]. That has stimulated and aided the progress of allosteric chemical systems on biomolecules.

A lot of the excellent works using DNA probes labeled by Q-dots (quantum dots) and Au nanoparticles have been the subjects of some precedent reviews. The DNA probing based on the simple FRET (Förster resonance energy transfer) between the organic dyes aligned on DNA were not covered in this review. The photochemically relevant DNA-based molecular systems selected here are categorized into three groups: (i) DNA-templated assemblies via hydrophobic and/or electrostatic interactions; (ii) DNA-directed metal complexation; and (iii) chemical transformation promoted on specific DNA molecules.

2. DNA as a nanomaterials template

Recently, DNA has received significant attention as a template for constructing several nanomaterials, because of its inherent structural order and polyelectrolyte character. In addition, the programmability of DNA in its lengths and sequences affords the production of well-defined 1D nanostructures.

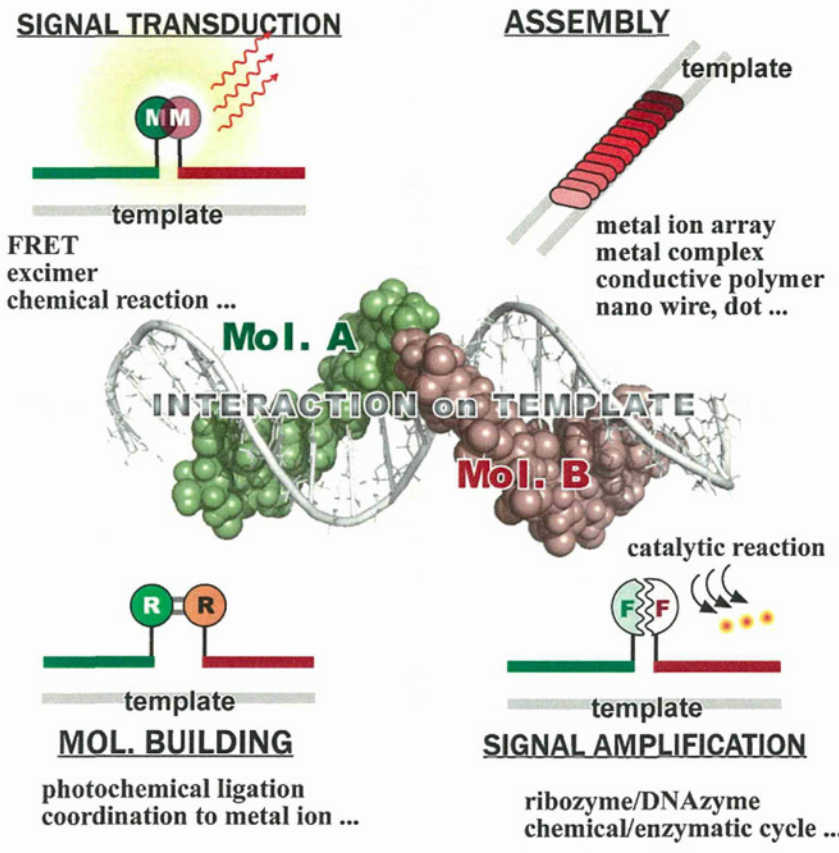

Fig. 1. Possible reactions promoted on DNA. DNA would be an excellent scaffold for various interactions or chemical reactions, if the systems are designed carefully. Genetic information is transduced to certain detectable signals by the synergistic functions of DNA complexes.

2.1. DNA-templated molecular/ion assemblies

2.1.1. Assemblies of organic dyes and metal complexes

Several small molecules are known to assemble along the DNA double-helix. For example, helical assemblies of fluorescent dyes [19–21] (Fig. 2a) and copper complexes [22](Fig. 2b) have been reported to form assemblies around the double-stranded DNA in a reversible manner. The binding modes of these molecules are thought to be groove binding and outside stacking, respectively. The optical properties of the assemblies are significantly affected by the feeding ratio (DNA:dye or metal complex) and DNA structure. DNA has been used as a scaffold to form site-selective arrays of porphyrins that are tethered to nucleobases. The assemblies permit electronic tuning of the resulting nanostructures [23,24].

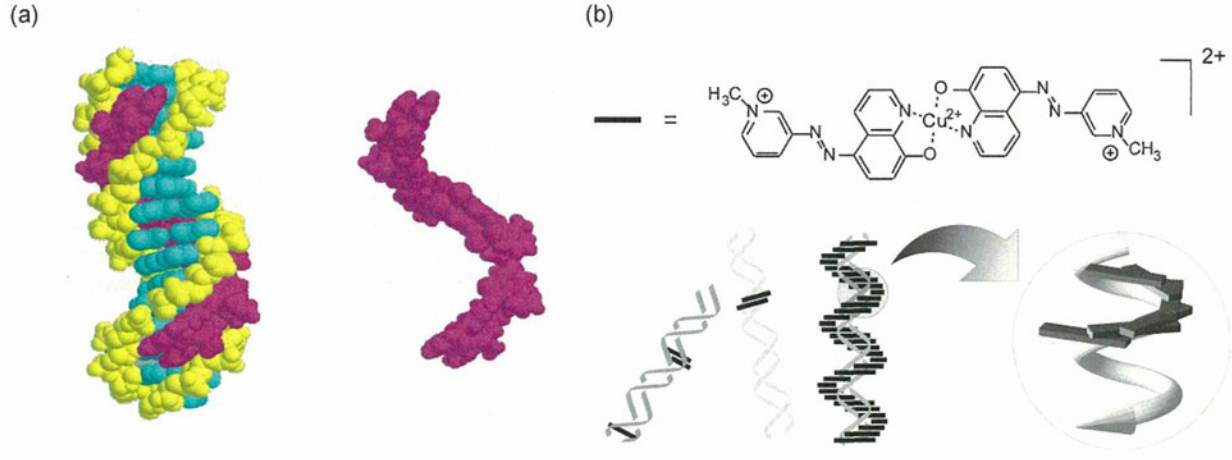

Fig. 2. (a) Molecular model showing three cyanine dye dimers aligned end-to-end within the minor groove of a DNA template (left). The DNA is removed in the figure on the right to better visualize the helical structure of the dye aggregate. DNA backbone, yellow; DNA base-pairs, cyan; cyanine dyes, magenta (reprinted from [19] with permission from the American Chemical Society). (b) The structure of the Cu^{2+} complex and its aggregate. Two ligands, which consist of an oxine and a pyridinium group, coordinate to a Cu^{2+} to give a stable dimer. The Cu^{2+} complex distributes on excess DNA in a highly biased manner because of cooperativity; that is, the Cu^{2+} complex assembles along either groove of the DNA to give a 1D spiral aggregate in which the long axis of each Cu^{2+} complex orients nearly perpendicular to the helix axis of the DNA duplex.

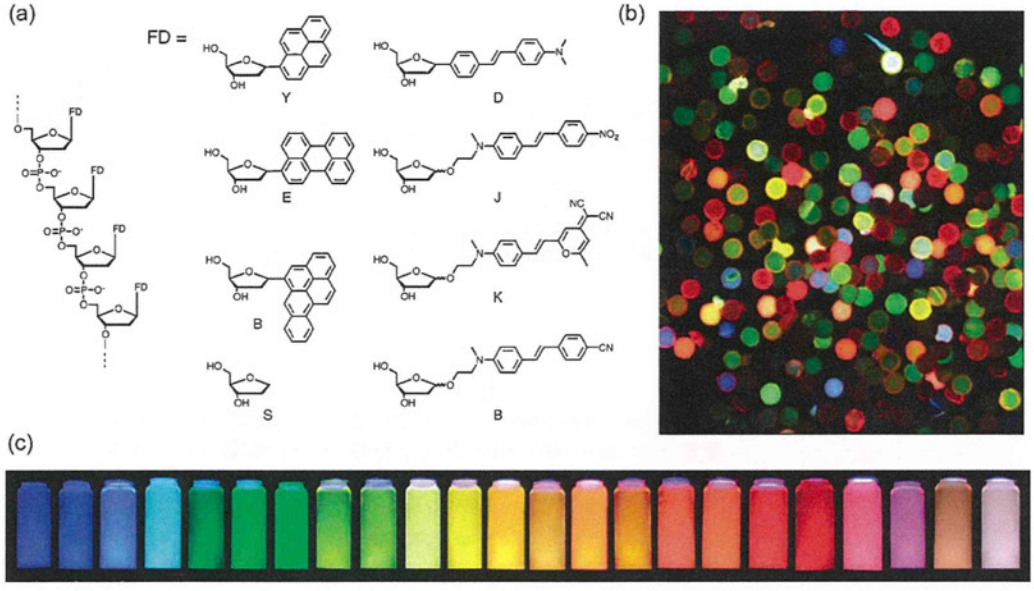

Fig. 3. (a) Typical structure of a fluorescent oligodeoxyriboside and its components. (b) Image from 4096-member tetramer library on PEG–polystyrene beads, taken with 340–380 nm excitation. The library contains all possible combinations of the eight monomers in (a) (reprinted from [27] with permission from the American Chemical Society). (c) Combined photograph of 23 fluorescent oligodeoxyribosides dissolved in phosphate buffer. The solutions were excited by a UV transilluminator (λ_{ex} = 354 nm) and the concentrations were adjusted to show relative colors at a similar brightness. These oligodeoxyribosides contain combinations of only four different chromophores (Y, E, B, K) (reprinted from [27] with permission from the American Chemical Society).

The DNA-directed clusters of various other chromophores such as pyrenes and perylenes have been reported [25–30]. For example, Kool and co-workers chose the unique chromophores' arrays as fluorescent metal ion sensors by screening from a random library [27,28] (Fig. 3). Asanuma and co-workers [29] and Garo and Häner [30] rationally designed the chromophores' arrays to form wavelength-tunable fluorescent tags and a light-harvesting antenna molecule, respectively.

As an assembly with larger dimensions, positively charged fullerene molecules were clustered on a negatively charged 2D-DNA lattice by coulombic forces and modulated as pear-like arrays by the alignment of the DNA scaffold [31].

2.1.2. Metal ion arrays on DNA

DNA has several types of Lewis bases that selectively coordinate to various metal ions. Silver ions electrostatically bound to DNA phosphate groups are chemically reduced to form metal nanodots that serve as nucleation sites for the formation of metallic nanowires along the length of the templated DNA [32–34]. This approach has been extended to the formation of bimetallic (Ag/Au) nanowires [35]. DNA-templated silver nanoclusters represent a new class of fluorophores [36–39]. The clusters are smaller than semiconductor quantum dots and have better photostability and brightness than commonly used organic dyes (Fig. 4). They have been used in chemical sensors [40,41], a hybridization assay [42], and cellular imaging [43]. Recently, copper nanoparticles were prepared using double-stranded DNA as the template. The particles showed unique fluorescent properties [44]. Fluorogenic assays for $Pb^{2+}$and ATP were performed using DNA-Cu nanoparticle complexes [45,46].

Natural and artificial nucleobases coordinate to specific metal ions (e.g., Ag^+, Cu^{2+}, Hg^{2+}) to form controlled metal ion arrays through the DNA axis [47–52]. For example, Tanaka et al. constructed selected metal ions' arrays with discrete numbers inside artificial DNA duplexes composed of chelating bases [50]. Ono and co-workers showed quantitative and specific formation of metal ion-mediated base-pairs, C–Ag^+–C and T–Hg^{2+}–T [51] (Fig. 5a). Ihara et al. reported that Ag^+ significantly stabilizes the triple-helix structure by forming a Ag^+-mediated base triplets, CG–Ag^+–C [52] (Fig. 5b). Among these systems, the Hg^{2+} and Ag^+ arrays have been applied to chemical sensors by combining with the signaling techniques based on FRET, DNAzyme catalytic reactions, and electrochemiluminescence [53–56].

2.2. DNA-templated polymerizations

The genetic code on DNA is copied to the daughter strand by DNA polymerase. DNA can also be used as the template for preparing functional polymers in the absence of enzymes. Several research groups have shown that the synthetic monomers containing nucleobases can be polymerized on the template DNA. Orgel and co-workers pioneered the research field by developing 2-methylimidazole-activated phosphate-coupling chemistry [57]. Lynn and co-workers [58] and Liu and co-workers [59] conducted the task using DNA-templated reductive amination. Using this approach these research teams produced oligomers of a defined length and sequence that were dependent on the templates.

Metal wires conduct electricity very well, but their conductance is not controllable. That would restrict the application of the metallic nanowires. On the other hand, like conventional silicon semiconductors, the electrical conductivity of conducting organic polymers can be reversibly tuned over several orders of magnitude. In addition, conducting polymers such as polyaniline (Pani) have mechanical flexibility and environmental stability, which makes them an ideal choice of materials for nanoelectronic devices. Pani is usually prepared by oxidizing the aniline monomer either electrochemically or chemically under strong acidic conditions. The harsh conditions preclude the use of delicate biomolecules as templates. The enzyme horseradish peroxidase (HRP) has been successfully employed as a catalyst for the polymerization of phenols and anilines. This enzymatic approach, involving mild reaction conditions, has opened the possibilities for DNA as a template. For example, Samuelson et al. succeeded in polymerization of anilines on a DNA template to form Pani under mild pH conditions (pH 4.3). In this process, anilinium ions that have bound electrostatically to the negatively charged phosphate groups of the DNA

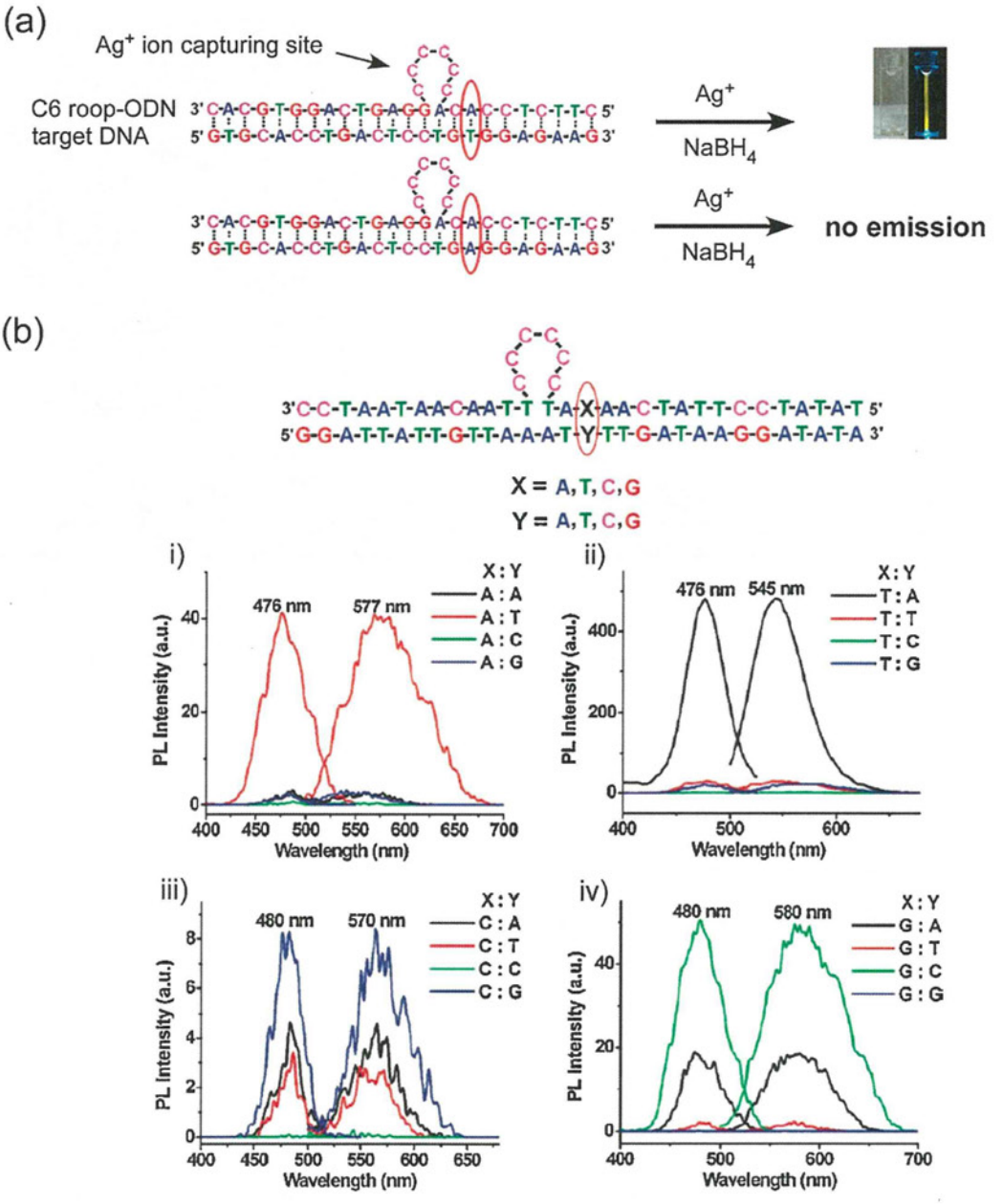

Fig. 4. (a) Sequence-dependent formation of fluorescent silver nanoclusters. Duplexes with inserted cytosine loops working as synthetic scaffolds to generate fluorescent silver clusters for the identification of the target DNA. (b) Photoluminescence (PL) spectra of silver nanoclusters obtained using the C6 loop-ODN/target DNA duplex as the scaffold with Y = A, T, C, G, and X = (i) A, (ii) T, (iii) C, and (iv) G. Measurements were carried out in 20 mM phosphate containing 1 mM magnesium acetate (pH 7.0). The concentration of the C6 loop-ODN/target DNA was 2 μM (Ag^+/duplex = 6:1; $NaBH_4/Ag^+$ = 1:1; reaction time, 7 h).
Reprinted from [36] with permission from the American Chemical Society.

backbone were converted to Pani by the reaction with HRP and H_2O_2. The phosphate-based template provides the requisite local environment to facilitate the para-directed coupling of the aniline molecules (Fig. 6). The wrapping of Pani on DNA has been found to induce a reversible change in the secondary structure of DNA [60]. Simmel and co-workers showed that DNA-templated Pani could also be prepared by ammonium persulfate as an oxidant or by the use of a ruthenium complex as photo-oxidant [61]. Pike and co-workers prepared unique nanowires of pentynyl-modified poly 2-(2-thenyl)-pyrrole on a DNA template. The polymer was subjected to further functionalization via click chemistry [62].

The polyioncomplex, DNA/Pani, however, has the propensity to agglomerate when it is immobilized on a substrate. He et al. circumvented this problem by template polymerization on stretched DNA on a Si surface. The conductivity of the Pani nanowire bridging the electrode gap was sensitive to the proton doping-undoping process [63].

Schuster et al. have tried to transfer the information of the templates such as the sequences and the lengths to the conducting polymers. They succeeded in preparing the Pani with a distinct length using monomers covalently modified to nucleobases. They prepared an oligonucleotide (ODN) carrying cytosines modified with aniline on its 4-amino group (exocyclic amino group). In the B-form DNA duplex, the aniline groups were found to regularly protrude into the major groove of the duplex. The obtained oligomers showed reasonable optical features depending on their lengths and the state of proton doping [64] (Fig. 7). This strategy was applied to the synthesis of polymers with mixed sequences consisting of

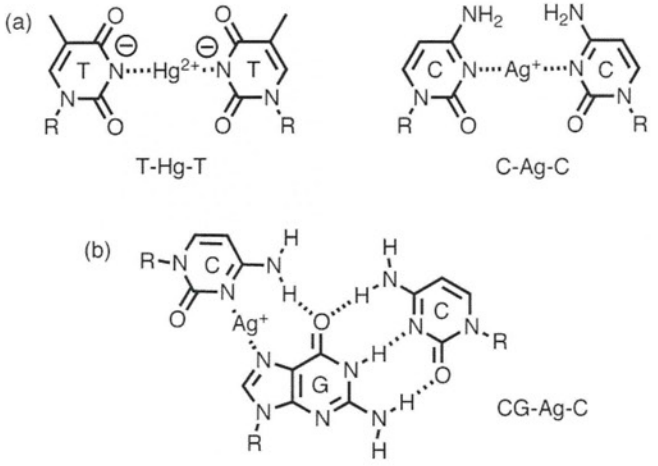

Fig. 5. (a) Metal-base pairs of two thymines with an Hg^{2+} ion (T–Hg^{2+}–T) and two cytosines with an Ag^{+} ion (C–Ag^{+}–C). (b) Hoogsteen base-pair-like Ag^{+}-mediated base triplet (CG–Ag^{+}–C) stabilizing a triple-helix DNA.

monomers other than aniline [65–67]. Recently, the same group reported the preparation of cyclic conducting oligomers consisting of six 2,5-bis(2-thienyl)pyrrole units using the technique of DNA-templated polymerization [68].

3. DNA-directed complexation

Structural programmability of DNA would provide an excellent microenvironment for molecular interactions. Several DNA conjugates carrying metal chelators have been synthesized. Chelators such as EDTA (ethylenediaminetetraacetic acid), DTPA (diethylenetriaminepentaacetic acid), IDA (iminodiacetic acid), Glu (glutamic acid), Phen (phenanthroline), Bipy (bipyridine), or Terpy (terpyridine) have been introduced to ODNs through covalent linking to their termini [69–74] or nucleobases [75,76], or built into the DNA backbone [77,78]. Under the conditions that provide particular DNA structures, the distance and mutual orientation of the two tethered chelators can be tuned and the complexes form (which would otherwise not occur in bulk solution) in a quantitative manner.

3.1. Metal ion-directed cooperative formation of specific structures

Ihara et al. tethered a chelator to one of the ends of an ODN. The two conjugates convergently bound to the duplexes with C_2 symmetric sequences through triple-helix formation. In these triplexes,

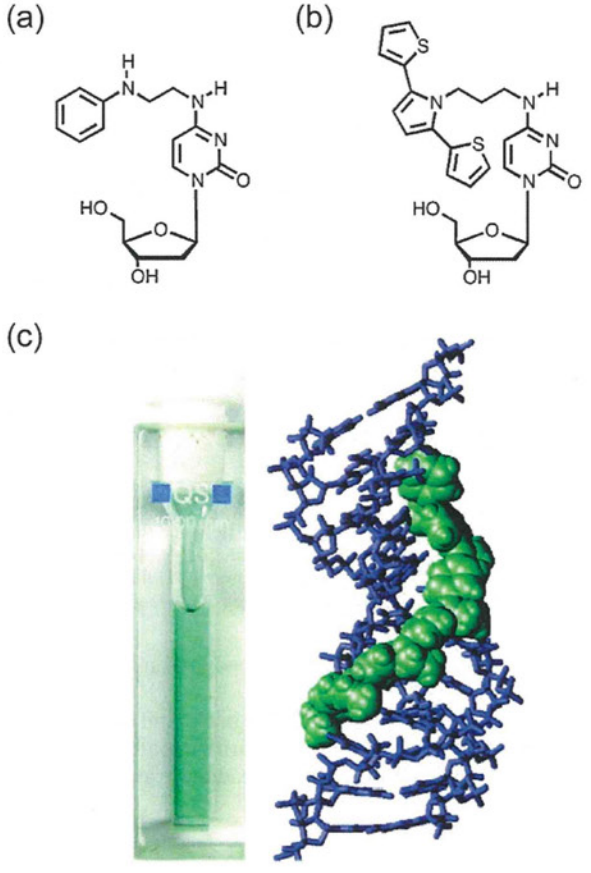

Fig. 7. Structure of (a) aniline-modified and (b) 2,5-bis(2-thienyl)pyrrole-modified monomers. (c) A structural model showing six aniline groups bonded head-to-tail conjoined to a DNA oligomer.
Reprinted from [64] with permission from the American Chemical Society.

the conjugates with IDA [69,70] and Glu [71] formed 2:1 complexes with a lanthanide or a copper ion, respectively, as the allosteric regulator. Secondary binding of the Glu–ODN conjugate to the half of the C_2 symmetric sequence was cooperatively enhanced by 165-fold in binding constant in the presence of Cu^{2+}. Krämer et al. modified two Terpys at the both ends of an ODN. The hybridization of the conjugate with the complementary sequence was regulated by reversible circularization through the formation of a 2:1 complex of Terpys at both ends of the conjugate with an appropriate metal ion such as Fe^{2+}, Cu^{2+}, or Zn^{2+} [72]. The release of Cu^{2+} and Zn^{2+} upon hybridization (linearization) led to the catalytic amplification of the

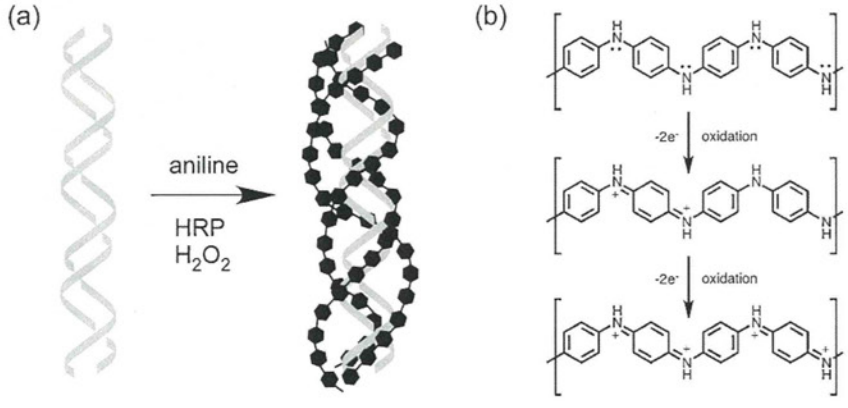

Fig. 6. (a) Schematic illustration of the formation of Pani on DNA. (b) Three oxidation states of Pani (from top to bottom: leuco, emeraldine, and pernigraniline oxidation states).

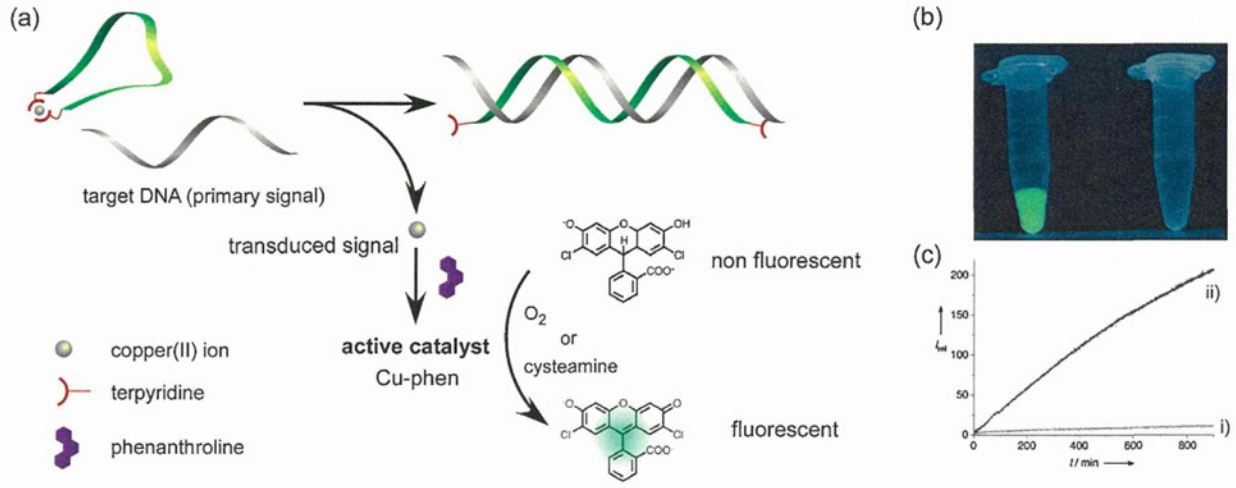

Fig. 8. (a) Detection of target DNA (primary signal) by allosteric signal transduction followed by catalytic amplification of the fluorescent signal. (b) Reaction solutions containing Terpy-modified ODN in the presence (left) and the absence (right) of the target DNA under UV light. The samples (2 μM Terpy-modified ODN, 2 μM target ODN, 10 μM 2′,7′-dichlorodihydrofluorescein, 5 μM Phen, 0.5 μM $CuSO_4$ and 100 μM cysteamine) were incubated for 12 h in 10 mM 3-(*N*-morpholino)propanesulfonic acid (MOPS) buffer containing 0.1 M NaCl at 25 °C (reprinted from [73] with permission from Wiley-VCH Verlag GmbH & Co. KGaA). (c) Increase in the relative fluorescence intensity with time: (i) Terpy-modified ODN, (ii) Terpy-modified ODN + target DNA (reprinted from [73] with permission from Wiley-VCH Verlag GmbH & Co. KGaA).

fluorescence signal by chemical and enzymatic reactions, respectively [73,74] (Fig. 8).

Terpy and Phen were built into the backbone of DNA oligomers by Sleiman et al. The conjugates formed particular structures that were dependent on the kinds of added transition metal ions according to the selectivity [77]. They reported the preparation of DNA complexes with a chiral metal–DNA junction with four different single-stranded arms [78]. This four-arm metal–DNA junction would be important in the area of DNA nanotechnology because it provides an effective building block that can be adapted to the

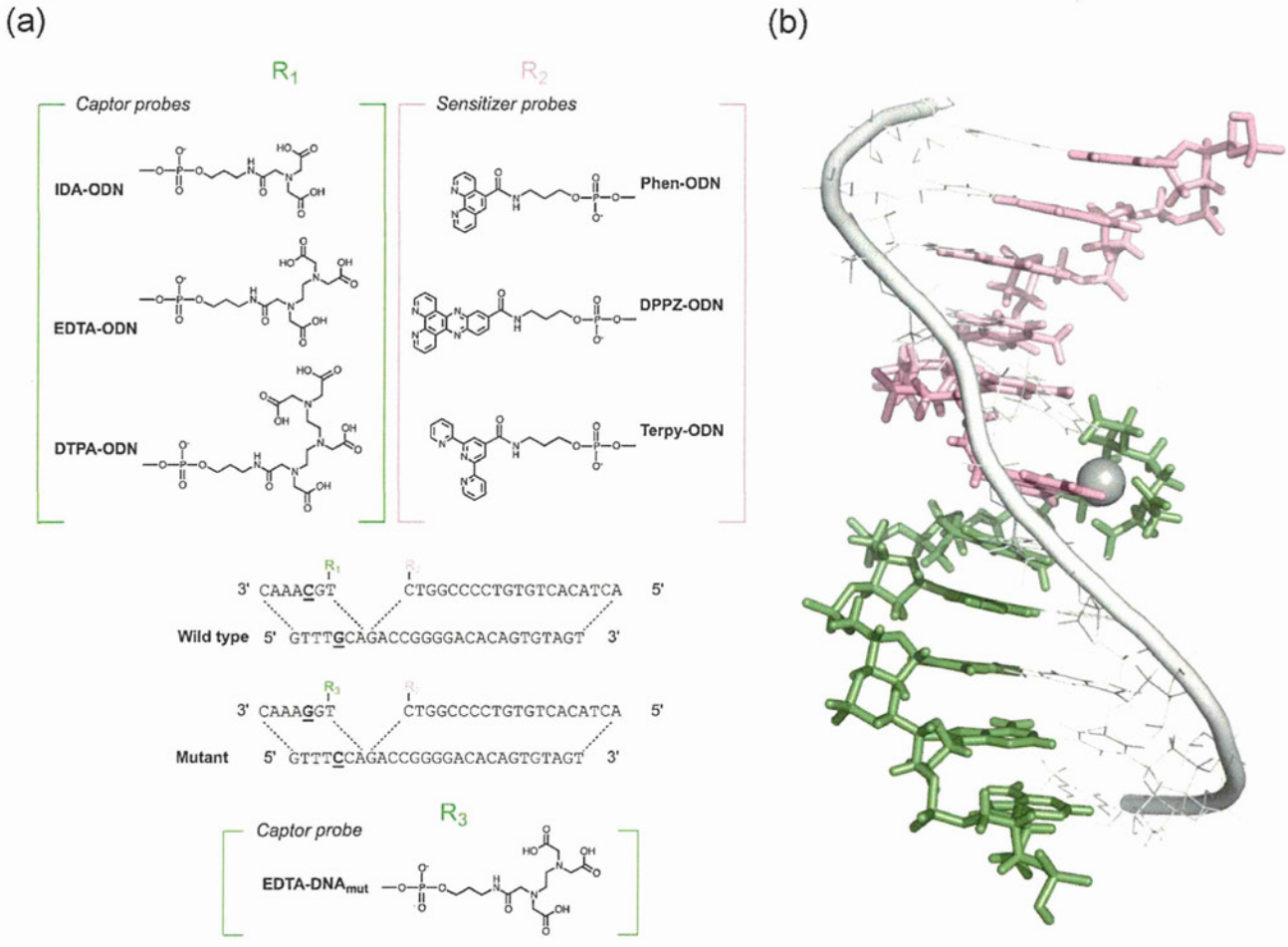

Fig. 9. (a) Sequences of the probes and targets. The wild-type and mutant are the 27-mer sequences of the TPMTgene containing one of the hot spots. (b) One of the possible structures of the ternary duplex consisting of Phen–ODN, EDTA–ODN and target DNA with Ln^{3+}.

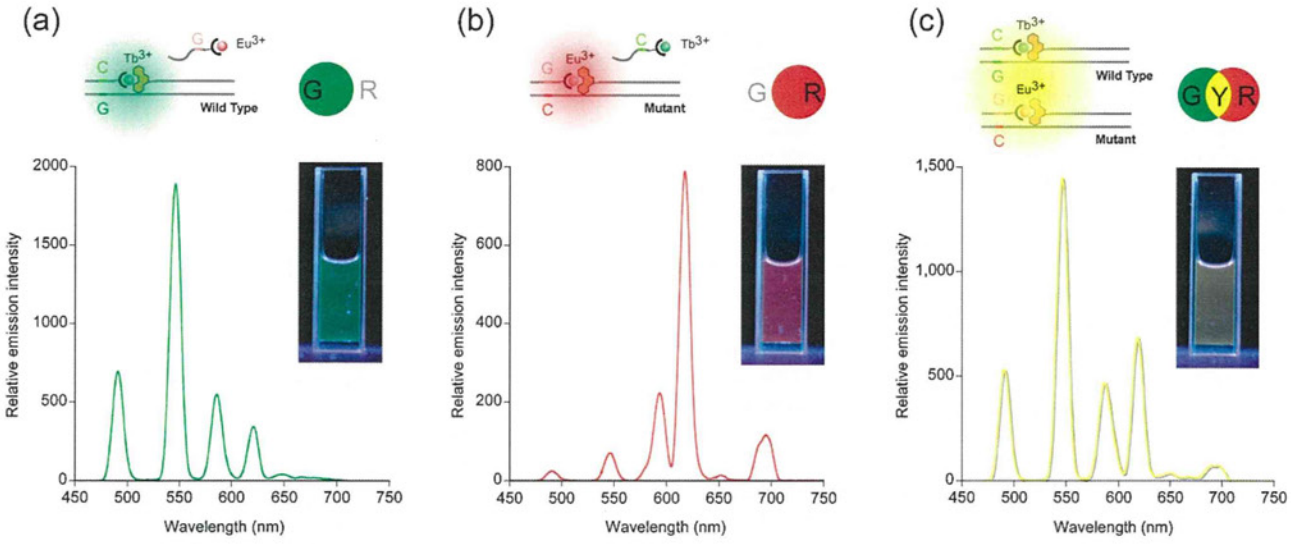

Fig. 10. SNP genotyping of the TPMT gene through the formation of a cooperative complex between the allele specific probes (Tb^{3+}/EDTA–ODN and Eu^{3+}/EDTA–ODN_{mut}) and the Phen–ODN on the targets. The emission spectra were collected in the presence of (a) wild-type, (b) mutant, and (c) wild type + mutant. All measurements were carried out in buffered solution (10 mM HEPES containing 1.0 M NaCl, pH 7.0) at 0 °C. The concentrations of each component for the ternary duplexes were 1.0 μM (except for solution (c), which contained 2.0 μM Phen–ODN). Inset: luminescence images of the each solution at 5 °C. Excitation source: low-pressure mercury lamp (6 W).
Reprinted from [82] with permission from Elsevier.

construction of a number of different 3D metal–DNA structures and networks.

3.2. Binary probing through metal ion complex formation

Binary probing is a smart strategy providing high selectivity [15,79]. Ihara et al. described the formation of luminous lanthanide complexes upon hybridization of split probes (binary probe) [80–83]. They prepared a series of DNA conjugates carrying a metal chelator at the terminus. Among the conjugates, they found that the combination between Phen– and EDTA–ODN was quite effective for DNA probing. Both conjugates convergently hybridized to the adjacent sites of the target DNA to form a tandem duplex (Fig. 9). The moieties of Phen and EDTA provided an appropriate cavity to accommodate a luminous lanthanide ion such as Tb^{3+} or Eu^{3+}, but only in the presence of the cognate targets. The long-lived luminescence (~ms) of the lanthanide complexes enables thorough reduction of background signals using time-resolved techniques in signal acquisition [80]. They showed that multi-color allele typing was possible by simultaneous use of both ions (Tb^{3+} and Eu^{3+}) [81,82] (Fig. 10). In an assay using the model sample of TPMT (thiopurine S-methyltransferase) gene, wild-type homozygote, mutant homozygote, and the heterozygote could be differentiated by the luminous colors of green (the color of Tb^{3+}), red (Eu^{3+}), and yellow ($Tb^{3+} + Eu^{3+}$), respectively. The luminous signal was affected not only by the rate of probe binding (the difference in thermal

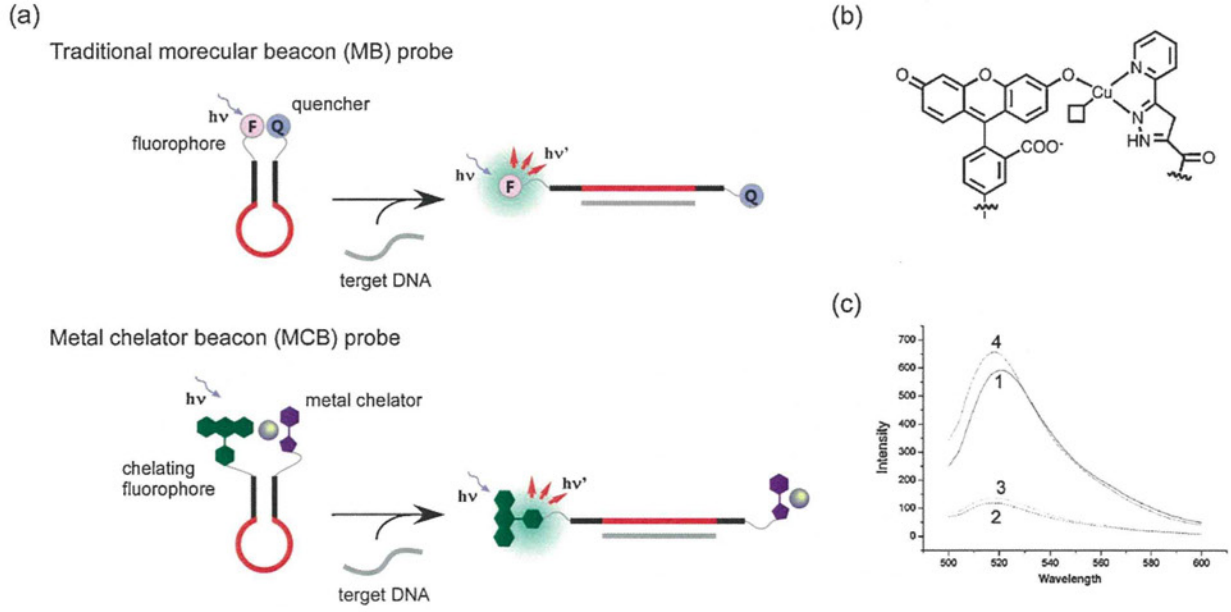

Fig. 11. (a) Schematic illustrations of fluorescence recovery based on traditional molecular beacon (MB) and metal chelator beacon (MCB) probes. (b) Structure of the intramolecular fluorescein complex with Cu^{2+}. (c) Relative fluorescence intensities of (1) MCB, (2) MCB + Cu^{2+}, (3) MCB + Cu^{2+} + single base mismatched DNA and (4) MCB + Cu^{2+} + full-matched DNA (reprinted from [87] with permission from the American Chemical Society). The measurements were carried out in 10 mM MOPS buffer containing 0.1 M NaCl, pH 7.0 at 25 °C. The concentrations of MCB, Cu^{2+} and target DNAs were 0.1 μM, 5 μM and 0.5 μM, respectively.

stability) but also by the local structural disruption induced by mispairing in the duplexes between the target and split probes [83]. This represents a novel nucleobase-discriminating principle, in which the split probes bind to all targets tightly, yet still the luminescence signal profile retains sequence selectivity. The system can be operated at a constant temperature regardless of the sequences of the targets as long as the temperature is lower than the melting temperature of the duplexes.

Krämer et al. prepared a set of two PNA (peptide nucleic acid) conjugates. One conjugate contains a Cu^{2+} complex and the other possesses a carboxylate linker that can be hydrolyzed by the metal. When the two probes bind adjacently to a DNA template, the two auxiliary groups are in close proximity and the linker is cleaved, releasing the carboxylate [84–86]. The reaction turned over and amplified the cleavage product. Added DNA analyte was regarded as a catalyst and the turnover numbers were observed to be up to 35 [85]. A single mismatch reduced the initial cleavage rate up to 100-fold [86]. They also proposed a new type of DNA MB carrying a Cu^{2+} complex and fluorescein on opposite ends of the DNA. The working principle is based on the reversible coordinating interaction of both auxiliary groups. Fluorescence was quenched by coordination of the hydroxyl group in fluorescein to the Cu^{2+} complex when the DNA formed a hairpin. The signal was restored by breaking the coordination on duplex formation with the addition of a suitable DNA sample [87] (Fig. 11).

4. Chemical transformations accelerated on DNA

The location, distance, and mutual orientation of the modified chemical groups on DNA can be tuned by taking advantage of the programmability of DNA structures. In this section, the chemical reactions concomitant with covalent bond formation and/or breaking that are promoted on DNA scaffolds are presented. There is a wide range of functional group-specific orthodox chemical reactions that take place under physiological conditions (ambient temperature in water at neutral pH). For example, amines and thiols selectively couple with succinimide esters and maleimides, respectively [88]. In addition, several bioorthogonal reaction pairs such as azide–alkyne, azide–phosphine, and tetrazine–alkene have been proposed [17]. The reactions are particularly important for in cell chemistry. The reactive components of the pairs are not found in nature, and therefore, the labeled molecules exclusively couple only with their own reaction partners. Nonetheless, the orthodox reactions are very useful, because of their higher reactivity. Orthodox reactions work well in the microenvironment provided by a DNA scaffold, because the reaction partners are positioned in close proximity to each other.

4.1. Fluorophore formation

4.1.1. Azide–phosphine reactions (Staudinger reactions)

The Staudinger reaction is the reaction between an azide and phosphine, which form a reactive aza-ylide as an intermediate that is hydrolyzed spontaneously to give a primary amine and a phosphine oxide [89,90] (Fig. 12). Saxon and Bertozzi modified the reaction to make it rather useful for connecting molecules with an amide bond linker [91]. The ester group on the phosphine traps the aza-ylide intermediate by intramolecular cyclization followed by hydrolysis. This Staudinger ligation reaction has found extensive applications for peptide ligation both in vitro and in vivo [92] (Fig. 13).

Taylor et al. has applied the reaction to DNA analysis. The phosphine was modified to fluorescein through an ester bond to form profluorescent (caged) fluorescein. The fluorescein was tethered to one end of a PNA pair. The azidoacetic acid was modified at the

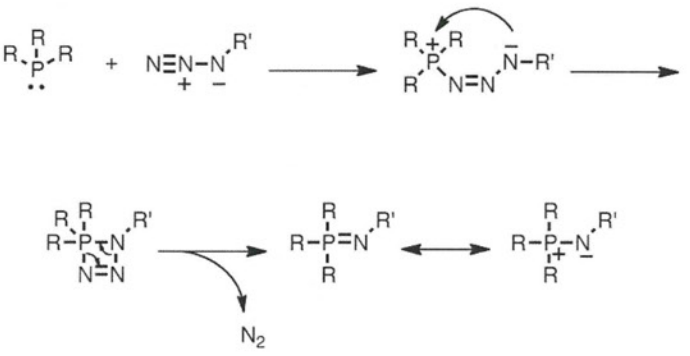

Fig. 12. Mechanism of the Staudinger reaction.

end of another PNA. The sequences of the two PNAs were designed to bind to adjacent sites of the target DNA so that their auxiliary groups were juxtaposition. Upon the addition of the target, the Staudinger ligation between the two PNAs was significantly accelerated to form the uncaged fluorescent fluorescein [93] (Fig. 14). However, spontaneous partial phosphine oxidation could not be avoided in biologically relevant conditions. To improve the fluorescence signal contrast, Winssinger et al. and Abe et al. used azide reduction instead of phosphine oxidation as the working principle for uncaging. The caged coumarin [94], rhodamine [95,96], and fluorescein [97] by the azide group were attached to one of the probes. Phosphine or dithiothreitol were tethered to the end of another probe as the reducing agent. The systems were applied to imaging of RNAs in live cells [95–97] and intron lariat RNA [98] (Fig. 15).

Leumann et al. used homo-DNA as the body of the binary probes based on the Staudinger reaction between rhodamine azide and phosphine. Homo-DNA is composed of glucopyranosyl nucleosides linked in a 4′-6′-fasion via phosphodiester bonds. Hybridization of homo-DNA is orthogonal to that of DNA. That is, while homo-DNA retains most of all hybridization properties, there is no cross-pairing between homo-DNA and natural DNA or RNA. DNA sensing

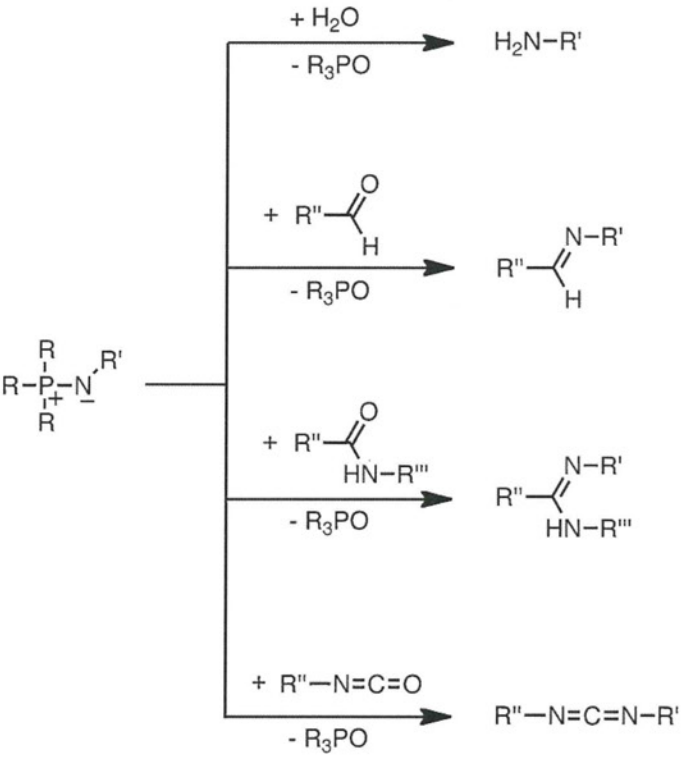

Fig. 13. The aza-ylide intermediated reaction with several electrophiles.

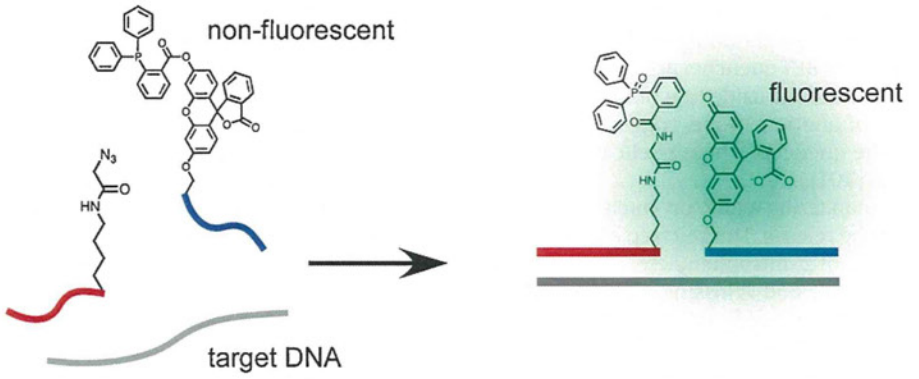

Fig. 14. Schematic illustration of DNA-triggered fluorescent probe activation by the Staudinger reaction.

was carried out by combining the techniques of MB. They prepared chimeric homo-DNA/DNA MB in which the DNA loop domain is responsible for analyte recognition, whereas the homo-DNA stem domain is used in signal generation [99]. This approach made the design of MB easier and contributed to a reduction in false positive signals and therefore improved signal contrast [100].

Kool et al. presented a versatile probe design for templated fluorescence activation based on quencher-release by

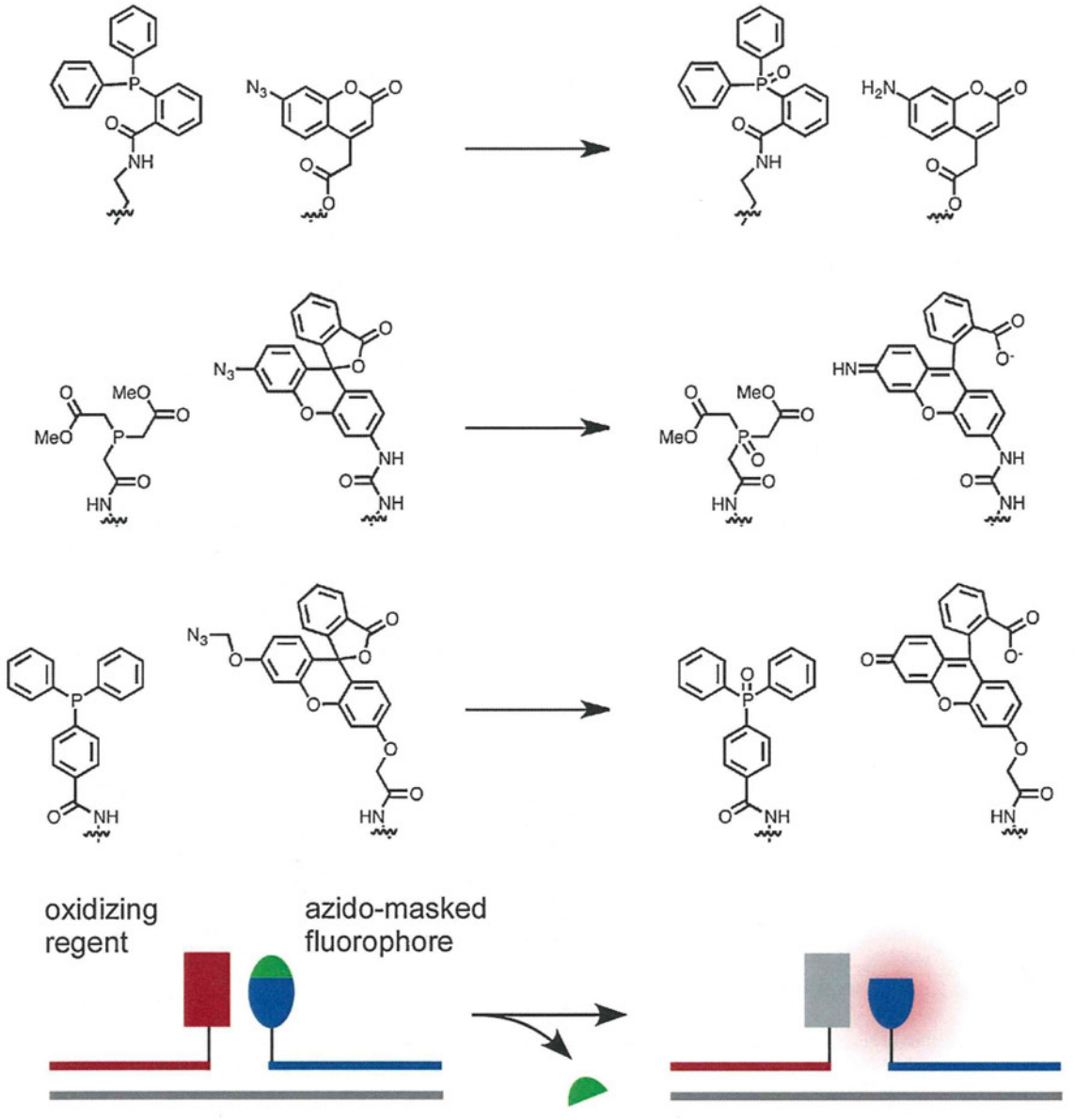

Fig. 15. DNA-templated activation of several azido-masked fluorophores by the Staudinger reaction.

Staudinger reductions. The quenched Staudinger-triggered α-azidoether probes are fluorophore-containing DNA probes whose fluorescence is deactivated by a FRET quencher attached through an α-azidoether linker. Reduction of the azide functionality, by phosphine tethered to the end of another probe, triggers cleavage of the linker and release of the quencher, thereby eliciting a robust fluorescence turn-on signal [101].

Taylor et al. reported pioneering work on nucleic acid triggered catalytic drug and probe release. The key step of the reaction was the orthodox hydrolysis of *p*-nitrophenylester by imidazole on DNA [102,103]. Robillard et al. and Winssinger et al. reported a technique of DNA-templated release of functional molecules with an azide-reduction-triggered immolative linker. They introduced a *p*-azidobenzyl group into the linker chain connecting the PNA and the functional molecules. Upon addition of the template DNA, the azide moiety is reduced by the phosphine modified on another probe to give a *p*-aminobenzyl group, which has immolative properties [104], and subsequently the functional molecules are released [105,106]. This approach represents a general prodrug design that releases the drug in the presence of target DNA or RNA.

4.1.2. Aldol-type reactions

Aldol reactions are very important in organic reactions, providing a good way to form carbon–carbon bonds. Usually they are carried out under anhydrous conditions. Aldol condensations are also well known in biochemistry. Aldolase is the enzyme that catalyzes analdol reaction. Class I aldolases utilize the ε-amino group of a Lys residue in the active site to form a Schiff base with one of the substrates, which activates the substrate as an aldol donor. Class II aldolases are Zn^{2+}-dependent metalloenzymes that facilitate enolate formation by coordination to the substrate's carbonyl oxygen. Barbas and co-workers [107] and Famulok and co-workers [108] have obtained efficient catalytic antibodies and ribozymes that were modeled after the class I and II aldolases, respectively. Oberhuber and Joyce succeeded in DNA-templated aldol reactions [109]. A glyceraldehyde and a glycolaldehyde tethered to the end of ODNs coupled to form a pentose on the DNA template by specific cross-aldol reaction in the presence of Lys. Tang and Marx reported an aldol reaction using a proline-modified ODN as the catalyst [110]. Li and co-workers reported that double-stranded DNA of natural origin could be used to facilitate the Henry reaction (nitro-aldol reaction) [111].

The works presented above indicates that aldol reactions can be used to prepare specific compounds in aqueous solution under mild conditions with the help of appropriate catalytic chemical groups, such as the enzymes use. The aldol condensation reaction was applied to the analyte-dependent synthesis of fluorescent reporter compounds. Hemicyanine dyes are generally synthesized by aldol-type condensations of heterocyclic quaternary salts bearing an active methyl group with aldehydes under anhydrous conditions. Huang et al. showed that hemicyanine dyes could be formed from nonfluorescent precursors. The two components of the aldol reaction (indolinium and aldehyde) tethered to the end of ODNs were assembled by designed duplex formation [112] (Fig. 16). The desired hemicyanine dye formed in the presence of a pyrrolidine derivative as a catalyst, which is well-known effective organocatalyst [113,114]. Matrices such as serum that are rich in primary amines and other nucleophiles did not affect the reaction yield of hemicyanine and its quantum yield. This reaction should be suitable to apply in a homogeneous fluorescent bioassay. Ladame et al. reported similar aldol-type reactions using the nonfluorescent precursors tethered to the ends of PNAs [115,116]. The reactions were performed on hairpin and G-quadruplex structures formed with appropriate DNA sequences. Expected cyanine dyes were generated in a "sequence + structure"-specific manner. The system worked at physiological pH and did not require the addition of explicit catalysts.

4.1.3. Azide–alkyne reactions (Huisgen reaction, click chemistry)

In 1963, the 1,3-dipolar cycloaddition between azides and acetylenes to yield triazoles was first described by Huisgen [117]. The reaction, however, required heating to obtain the triazoles in appreciable amounts. Recently, Sharpless et al. and Meldal et al. reported that Cu^{+} complexes acting as catalyst noticeably accelerated the reaction [118,119] (Fig. 17a). The reaction was found to proceed well in aqueous solution under physiological conditions. Because of its fast reaction kinetics and excellent functional group tolerance, it has been widely employed in biological studies and now widely referred to as "click chemistry" or CuAAC (copper-catalyzed azide–alkyne cycloaddition).

Komiyama et al. used the reaction for the identification of a G-quadruplex structure and discovered a DNA–RNA hybrid-type G-quadruplex structure formed by human telomeric DNA and RNA sequences [120]. Kitade et al. prepared an ODN modified with aryl acetylene as a versatile handle for labeling. They succeeded in quick and efficient labeling of benzylazide derivatives carrying ^{18}F for PET (positron emission tomography) probing by ligand-free CuAAC [121]. Jentzsch and Mokhir reported a fluorogenic, nucleic acid directed click reaction [122]. The method involves generating a fluorescent product from a nonfluorescent precursor, 4-ethynyl-1,8-naphthalimide [123] tethered to one of the probes, by clicking the fluorescent trigger, an azide group modified on a second probe. Using this click-activated fluorescent probe, they demonstrated the

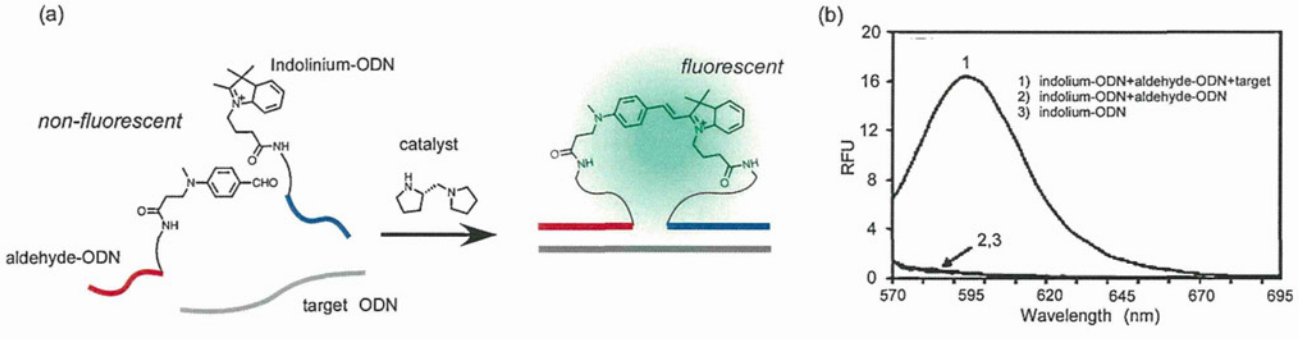

Fig. 16. (a) DNA-templated formation of fluorescent hemicyanine by an aldol-type condensation. (b) Relative fluorescent intensities of the reaction mixtures. The concentrations of reagent ODNs and target were 0.2 μM. The reaction was carried out in the presence of 10 mM (*S*)-pyrrolidine methylpyrrolidine in 50 mM sodium phosphate buffer containing 1 M NaCl, pH 8.4 at room temperature for 140 h.

Reprinted from [112] with permission from the American Chemical Society.

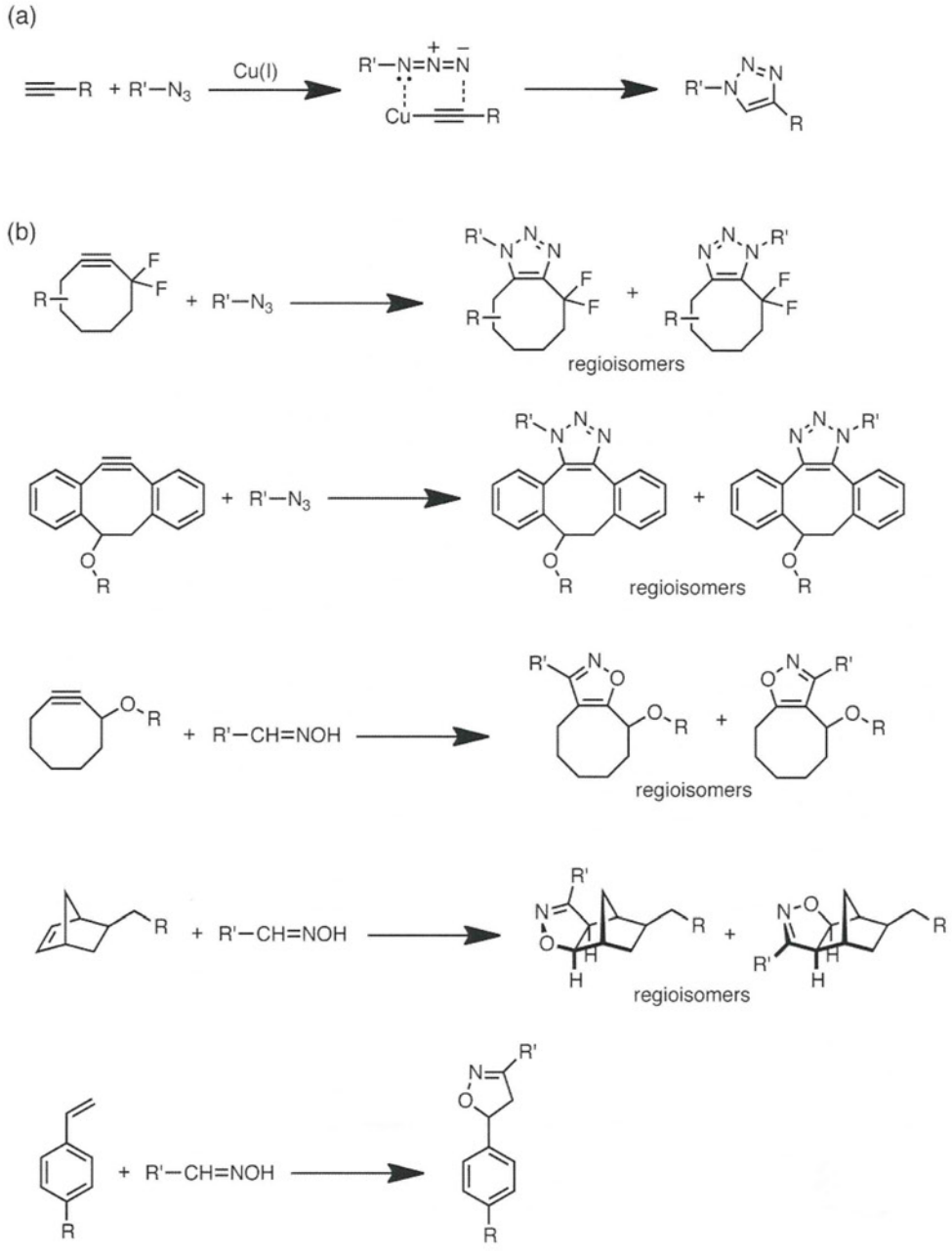

Fig. 17. (a) Cu(I)-catalyzed ligation of azides and terminal alkynes (click chemistry). (b) A variety of Cu(I)-free click chemistry reactions.

discrimination of an SNP (single nucleotide polymorphism) on a template DNA.

However, the application of CuAAC to cell and organisms is limited because of the toxicity of copper. To circumvent this drawback, several metal-free azide–alkyne cycloadditions have been developed (Fig. 17b). One approach was reported by Bertozzi et al. whereby they harnessed the ring strain in cyclooctyne that contributes to a significantly faster reaction rate [124,125] and called this reaction SPAAC (strain-promoted azide–alkyne cycloaddition). The rate was further improved by Boons and co-workers using an alternative strained cyclooctynein which two benzene rings were fused to give dibenzocyclooctyne (DIBO) [126]. To add versatility to the SPAAC, they masked the triple bond of DIBO as cyclopropenone to afford a photo-triggered reaction. The masked DIBO does not react with azides in the dark. The irradiation of the cyclopropenones provides efficient regeneration of the corresponding DIBOs that then undergo fast cycloaddition with azides [127] (Fig. 18). Taton and co-workers [129] and Filippov and co-workers [128] prepared a DIBO-modified ODN using DIBO phosphoramidite. The study showed that the DIBO group not only survived the standard acidic and oxidative conditions employed in solid-phase DNA synthesis, but that it also survived the thermal cycling and standard conditions used in PCR. As a result, PCR with DIBO-modified primers yielded "clickable" amplicons that could be tagged with azide-modified fluorophores or immobilized on azide-modified surfaces by SPAAC [129]. El-Sagheer and co-workers performed templated DNA strand ligation by SPAAC using fluorescently labeled ODNs [130]. The reaction was essentially complete in 1 min and inhibited by the presence of a single mismatched base-pair suggesting applications in genetic analysis.

Recently, several alternatives to azide or acetylene have been reported to improve the kinetics of the catalyst free 1,3-dipolar cycloaddition (Fig. 17b). For examples, Heaney et al. reported the modification of ODN with fluorophores via nitrile

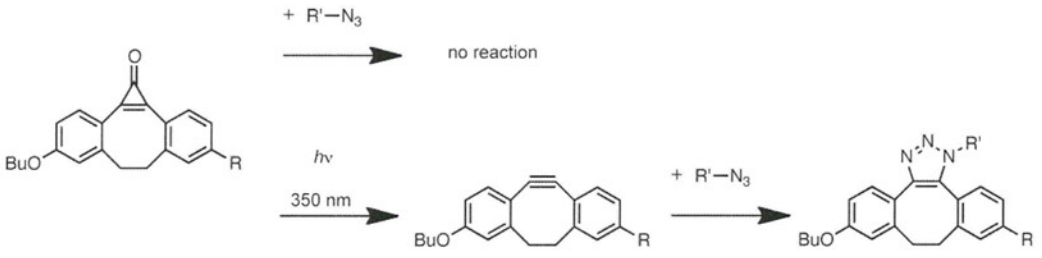

Fig. 18. Photochemical initiation of Cu(I)-free azide–alkyne cycloaddition.

oxide–cyclooctyne cycloaddition [131,132]. Carell and co-workers presented a DNA modification via a nitrile oxide–norbornene cycloaddition [133]. The reaction allows high-density functionalization of ODNs with a large variety of molecules directly onto solid supports and even in DNA synthesizers. They also presented a multistep sequential DNA modification using Cu-catalyzed and Cu-free click reactions [134].

4.1.4. Other types of reactions

Seitz et al. showed an approach for sensitive DNA analysis by DNA-catalyzed transfer of a reporter group. The DNA analyte acts as a template in the reaction of an iso-cysteine-mediated transfer of one of the molecules of a FRET pair. Dabcyl (4-[4-dimethylamino]phenylazo)benzoyl)transfer from one of the probes restored the fluorescein emission on the same probe while switching off the emission of rhodamine on the other probe that accepted the dabcyl [135,136] (Fig. 19). Organometallic activation of a fluorogen catalyzed by the DNA template (analyte) was performed by Kool et al. They prepared a pair of the probes bearing organomercury and caged rhodamine functionalities. The two DNA conjugates hybridized to adjacent sites on the template DNA and yielded a fluorescence signal arising from metal-assisted rhodamine uncaging [137]. Winssinger et al. reported a fluorescent DNA assay involving the uncaging of fluorophores by Ru^{2+} complex-catalyzed photoreduction with visible light [138]. Hermann et al. reported a unique fluorogenic reaction based on heavy-atom removal for ultrasensitive DNA detection. One of the probes was modified with BODIPY (boron-dipyrromethene, 4,4-difluoro-4-bora-3a,4a-diaza-*s*-indacene) quenched by iodine. The fluorescence of the BODIPY was restored by the Pd-catalyzed Heck reaction promoted using a DNA template [139]. Mokhir et al. presented a sensitive DNA analysis by autocatalytic chromogenic and fluorogenic photochemical reactions. The principle of these methods is based on the sequence-specific DNA strand displacement and concomitant restoration of the photosensitizer of the catalytic reactions [140–142] (Fig. 20). Willner and co-workers also reported sensitive DNA detection by amplification using a catalytic reaction through the autonomous assembly of a hemin/G-quadruplex DNAzyme nanowire [143].

4.2. Photocrosslinking

Several small ligands are well known to crosslink DNA strands in intra- and inter-strand manners. As classical crosslinking drugs,

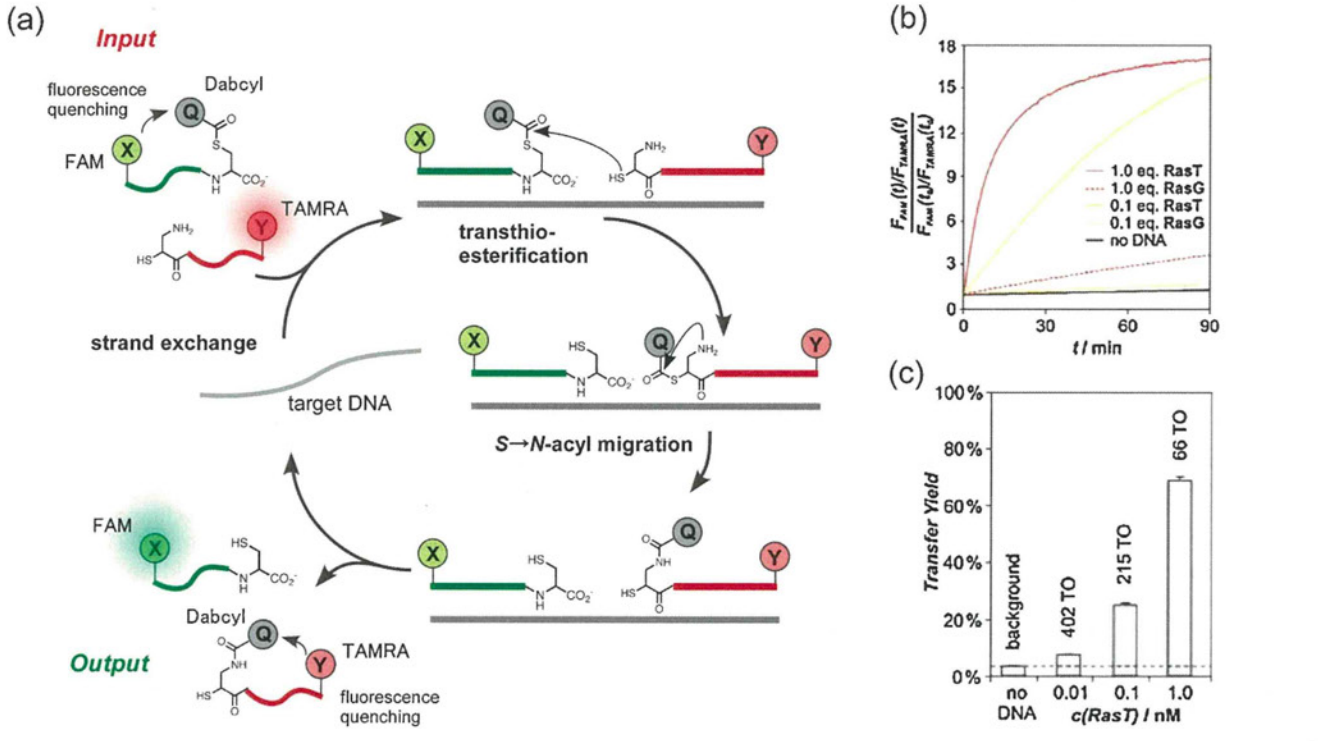

Fig. 19. (a) Catalytic cycle of DNA-assisted transfer of a quencher (Dabcyl: 4-[4-(dimethylamino)phenylazo]benzoyl) group from a FAM (6-carboxyfluorescein: λ_{ex} = 465 nm, λ_{em} = 525 nm)-modified probe to a TAMRA (5-carboxytetramethylrhodamine: λ_{ex} = 558 nm, λ_{em} = 593 nm)-modified one. (b) Time courses of relative F_{FAM}/F_{TAMRA} ratio at different RasT (matched target) and RasG (single-base mismatched target) concentrations. The reaction was carried out in 10 mM sodium phosphate buffer (pH 7.0) containing 200 nM probes, 200 mM NaCl, 0.2 mM TCEP, and 0.1 mg/mL Roche blocking reagent at 37 °C (reprinted from [135] with permission from the American Chemical Society). (c) Transfer yields after 24 h and turnover numbers (TO) (reprinted from [135] with permission from the American Chemical Society).

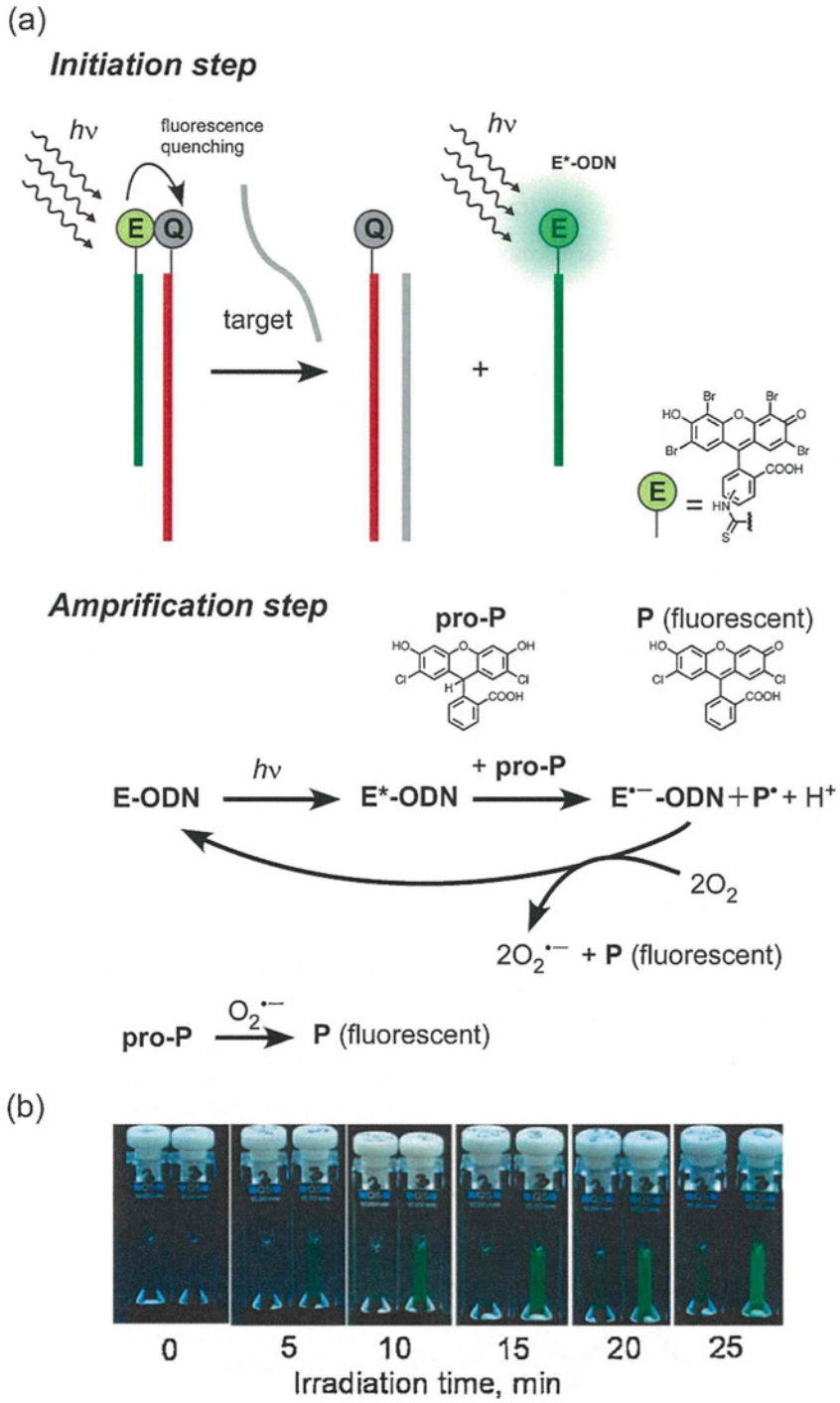

Fig. 20. (a) Schematic illustration of a nucleic acid-assisted autocatalytic photochemical reaction; E: eosin, Q: black-hole-quencher-3, pro-P: 2′,7′-dichlorofluorescin; P: 2′,7′-dichlorofluorescein (oxidation product of pro-P). (b) Naked eye detection of nucleic acids using the autocatalytic photochemical reaction of the oxidation of pro-P; photooxidation of pro-P (15 μM) was conducted for defined periods; left cuvette in each pair contains the E-ODN/Q-ODN duplex (0.2 μM) and right cuvette contains additionally target ODN (0.2 μM).

Reprinted from [140] with permission from The Royal Society of Chemistry.

cisplatin, nitrogen mustards, psoralens, and mitomycin C have been well characterized [144]. Some molecules are highly efficient as chemotherapeutic agents targeting nucleic acids. Moreover, some Pt(II) complexes are employed for the treatment of certain human cancers [145,146]. Since these initial studies, numerous efforts have been devoted to the development of efficient crosslinkers for DNA probing, DNA manipulation, and therapeutic applications. Some examples of crosslinkers based on photochemical reactions, photocrosslinkers, are presented here.

Psoralen is a planar, aromatic compound that intercalates into double-stranded nucleic acids. Upon irradiation of the complex with long wavelength UV light (UVA), psoralen adducts are made via cyclobutane formation with pyrimidine bases (Fig. 21). There have been many studies devoted to the development of psoralen derivatives over the last two decades. Recently Brown and co-workers tethered psoralen to the end of triplex-forming ODNs (Pso–TFO). UV irradiation of the triplexes containing Pso–TFO produced photoadducts at TpA